NASA COOPERATIVE AGREEMENT NCC1-112

STUDY OF THE TRANSITION FLOW REGIME

USING MONTE CARLO METHODS

Final Report

Prepared by

H. A. Hassan
Principal Investigator
Department of Mechanical and Aerospace Engineering
Campus Box 7910
North Carolina State University
Raleigh, North Carolina 27695-7910

During this period a presentation was made at the 7th AIAA/ASME Joint Thermophysics Conference. Another publication, dealing with turbulence at hypersonic Mach numbers, will be presented at the AIAA Aerospace Sciences meeting in January 1999. Copies of these publications are made part of this final report. In addition, progress made by Professor Bird is enclosed.

In addition, a list of published research conducted at N. C. State University and supported by the cooperative agreement is enclosed. It provides a list of students supported by the Cooperative Agreement.

Publications supported in part by NCC1-112

1. "Grid Generation and Adaptation for the Direct Simulation Monte Carlo Method", D. P. Olynick, J. N. Moss and H. A. Hassan, AIAA Paper 88-2734, June 1988, also *Journal of Thermophysics and Heat Transfer*, Vol. 3, pp. 368-373, October 1989.

2. "Influence of Afterbodies on AOTV Flows", D. P. Olynick, J. N. Moss and H. A. Hassan, AIAA Paper 89-0331, January 1989.

3. "Monte Carlo Simulation of Reentry Plasmas", A. B. Carlson, H. A. Hassan, and J. N. Moss, AIAA Paper 89-0683, January 1989.

4. "Study of Hypersonic Flow Past Sharp Cones", J. C. Taylor, J. N. Moss and H. A. Hassan, AIAA Paper 89-1713, June 1989.

5. "Direct Simulation of Reentry Flows with Ionization", A. B. Carlson and H. A. Hassan, AIAA Paper 90-0146, January 1990, also, *Journal of Thermophysics and Heat Transfer*, Vol. 6, pp. 400-404, July 1992.

6. "Monte Carlo Simulation of Vibrational Relaxation in Nitrogen", D. P. Olynick, J. N. Moss, and H. A. Hassan, AIAA Paper 90-1767, June 1990; Also, *Journal of Thermophysics and Heat Transfer*, Vol. 6, pp. 22-26, January 1992.

7. "Monte Carlo Simulation of Re-Entry Flows Using a Bimodal Vibration Model", D. P. Olynick, J. N. Moss, and H. A. Hassan, *Journal of Thermophysics and Heat Transfer*, Vol. 4, pp. 273-277, July 1990.

8. "Direct Simulation Monte Carlo with Ionization and Radiation", A. B. Carlson and H. A. Hassan, 17th International Symposium on Rarefied Gas Dynamics, Edited by A. E. Beylich, VCH, Weinheim, Germany, pp. 763-769, 1991.

9. "Monte Carlo Simulation of Nonequilibrium Shock Fronts", D. P. Olynick, J. N. Moss, and H. A. Hassan, AIAA Paper 91-1341, June 1991; Also, *Journal of Thermophysics and Heat Transfer*, Vol. 6, No. 4, pp. 626-630, Oct.-Dec. 1992.

10. "Radiation Modeling with Direct Monte Carlo", A. B. Carlson, and H. A. Hassan, AIAA Paper 91-1409, June 1991; Also, *Journal of Thermophysics and Heat Transfer*, Vol. 6, No. 4, pp. 631-636, Oct.-Dec. 1992.

11. "Radiation Transport Around Axisymmetric Blunt Body Vehicles Using a Modified Differential Approximation", Lin C. Hartung and H. A. Hassan, AIAA Paper 92-0119,

January 1992; Also, *Journal of Thermophysics and Heat Transfer*, Vol. 7, No. 2, pp. 220-227, April-June 1993.

12. "Monte Carlo Simulation of Reentry Flows with Ionization", Jeff C. Taylor, Ann B. Carlson, and H. A. Hassan, AIAA Paper 92-0493, January 1992.

13. "Monte Carlo Simulation of Entry in the Martian Atmosphere", David B. Hash and H. A. Hassan, AIAA Paper 92-0494, January 1992; Also, *Journal of Thermophysics and Heat Transfer*, Vol. 7, No. 2, pp. 228-232, April-June, 1993.

14. "Direct Simulation with Vibration-Dissociation Coupling", D. B. Hash and H. A. Hassan, AIAA Paper 92-2875, July 1992; also *Journal of Thermophysics and Heat Transfer*, Vol. 7, No. 4, pp. 680-686, Oct.-Dec. 1993.

15. "A New Two-Temperature Dissociation Model for Reacting Flows", D. P. Olynick and H. A. Hassan, AIAA Paper 92-2943, July 1992; also *Journal of Thermophysics and Heat Transfer*, Vol. 7, No. 4, pp. 687-696, Oct.-Dec. 1993.

16. "Direct Simulation of Diatomic Gases Using the Generalized Hard Sphere Model", D. B. Hash and H. A. Hassan, AIAA Paper 93-0730, January, 1993.

17. "A Generalized Hard-Sphere Model for Monte Carlo Simulation", H. A. Hassan and D. B. Hash, *The Physics of Fluids*, Vol. 5, No. 3, pp. 738-744, March 1993.

18. "Monte Carlo Simulation of Radiating Re-Entry Flows", Jeff C. Taylor, Ann B. Carlson, and H. A. Hassan, AIAA Paper 93-2809, July 1993; Also, *Journal of Thermophysics and Heat Transfer*, Vol. 8, No. 3, pp. 478-485, July-September 1994.

19. "Comparisons Between DSMC and Navier-Stokes Equations for Re-Entry Flows", D. R. Olynick, J. C. Taylor, and H. A. Hassan, AIAA Paper 93-2810, July 1993, Also, *Journal of Thermophysics and Heat Transfer*, Vol. 8, No. 2, pp. 251-258, April-June 1994.

20. "Monte Carlo Simulation Using Attractive-Repulsive Potential", D. B. Hash and H. A. Hassan, in *Rarefied Gas Dynamics: Theory and Simulations, Progress in Astronautics and Aeronautics*, edited by B. D. Shizzal and D. P. Weaver, Vol. 159, pp. 284-293, 1994.

21. "Effects of Chemistry and Rarefaction on Blunt Body Wake Structure", V. K. Dogra, R. G. Wilmoth, J. N. Moss, J. C. Taylor, and H. A. Hassan, AIAA Paper 94-0352, January 1994; Also, *AIAA Journal*, Vol. 33, No. 3, pp. 463-469, March 1995.

22. "Rates of Thermal Relaxation in Direct Simulation Monte Carlo Methods", B. L. Haas, D. B. Hash, G. A. Bird, F. E. Lumpkin, III and H. A. Hassan, *Physics of Fluids*, Vol. 6, No. 6, pp. 2191-2201, June 1994.

23. "Upwind·Methods for Ionized Flows", J. C. Taylor, D. R. Olynick, and H. A. Hassan, AIAA Paper 94-1957, June 1994.

24. "Rarefaction Effects on Blunt Body Wake Structure for Earth Entry Conditions", V. K. Dogra, J. N. Moss, R. G. Wilmoth, J. C. Taylor, and H. A. Hassan, AIAA Paper 94-2016, June 1994; Also, *Journal of Thermophysics and Heat Transfer*, Vol. 9, No. 3, July September 1995, pp. 464-470.

25. "Parallel DSMC Solution of Three-Dimensional Flow Over a Finite Flat Plate", R. P. Nance, R. G. Wilmoth, B. Moon, H. A. Hassan, and J. Saltz, AIAA Paper 94-2019, June 1994; Also, *Journal of Thermophysics and Heat Transfer*, Vol. 9, No. 3, July-September 1995, pp. 471-477.

26. "Direct Simulation of Diatomic Gases Using the Generalized Hard Sphere Model", D. B. Hash, J. N. Moss, and H. A. Hassan, *Journal of Thermophysics and Heat Transfer*, Vol. 8, No. 4, Oct.-Dec. 1994, pp. 758-764.

27. "A DSMC Navier-Stokes Hybrid Solver", David B. Hash and H. A. Hassan, AIAA Paper 95-0410, January 1995.

28. "The GHS Interaction Model for Strong Attractive Potentials", J. A. Kunc, D. B. Hash, and H. A. Hassan, *The Physics of Fluids*, Vol. 7, No. 5, pp. 1173-1175, May 1995.

29. "A Radiation Absorption Model for the DSMC Method", J. C. Taylor, H. A. Hassan, and L. Hartung Chambers, in *Rarefied Gas Dynamics 19*, J. K. Harvey and R. G. Lord, Editors, Vol. 2, 1995, pp. 829-835.

30. "Rarefaction Effects on Blunt-Body Wake Structure", V. K. Dogra, J. N. Moss, J. C. Taylor, D. B. Hash, and H. A. Hassan, in *Rarefied Gas Dynamics 19*, J. K. Harvey and R. G. Lord, Editors, Vol. 2, 1995, pp. 1154-1160.

31. "Direct Simulation of Shock Front Radiation in Air", A. K. Berghausen, J. C. Taylor, and H. A. Hassan, AIAA Paper 95-2051, June 1995; Also, *Journal of Thermophysics and Heat Transfer*, Vol. 10, No. 3, July-September, 1996, pp. 413-418.

32. "A Decoupled DSMC/Navier-Stokes Analysis of a Transitional Flow Experiment", D. B. Hash, and H. A. Hassan, AIAA Paper 96-0353, January 1996.

33. "A Comparison of Grid-Definition Schemes for DSMC", R. P. Nance, R. G. Wilmoth, and H. A. Hassan, AIAA Paper 96-0604, January 1996; also, *Journal of Thermophysics and Heat Transfer*, Vol. 11, No. 2, April-June, 1997, pp. 296-303.

34. "Assessment of Schemes for Coupling Monte Carlo and Navier-Stokes Solution Methods," D. B. Hash and H. A. Hassan, *Journal of Thermophysics and Heat Transfer*, Vol. 10, No. 2, April-June 1996, pp. 242-249.

35. "A Novel Approach for Calculating Equilibrium Radiating Flows," F. Brauns and H. A. Hassan, AIAA Paper 96-1887, June 1996; also, *Journal of Thermophysics and Heat Transfer*, Vol. 11, No. 1, January-March, 1997, pp. 52-58.

36. "Role of Boundary Conditions in Monte Carlo Simulation of MEMS Devices," R. P. Nance, D. B. Hash and H. A. Hassan, AIAA Paper 97-0375, January 1997; Also, *Journal of Thermophysics and Heat Transfer*, Vol. 12, No. 3, July-September 1998, pp. 447-449.

37. "Two-Dimensional Coupling Issues of Hybrid DSMC/Navier-Stokes Solvers," D. B. Hash and H. A. Hassan, AIAA Paper 97-2507, June 1997.

38. "Transition and Turbulence Modeling for Blunt-Body Wake Flows," R. P. Nance, T. J. Horvath, and H. A. Hassan, AIAA Paper 97-2570, June 1997.

39. "Solution of Transitional Wake Flows at Mach 10," R. P. Nance, B. R. Hollis, T. J. Horvath, and H. A. Hassan, AIAA Paper 98-2939, June 1998.

40. "Turbulence Modeling of Shock-Dominated Flows with a k-ζ Formulation," R. P. Nance and H. A. Hassan, AIAA Paper 99-0153, January 1999.

FINAL REPORT: 1 November 1997 to 31 October 1998

G.A. Bird

1. New DSMC Procedures

(a) Transient adaptive sub-cells

Several recent applications of the DSMC method have shown that unsteady two-dimensional flows can now be studied without resorting to ensemble averaging. For Knudsen numbers well under 0.01, this requires the flow output to be based on computational cells that are large in comparison with the mean free path. However, a basic requirement of the DSMC method is that the mean spacing between collision partners should be small in comparison with the local mean free path. The two requirements can be reconciled by the specification of a large number of sub-cells in each cell. Sub-cells are required only by the collision routine and the latest DSMC programs employ 'transient' sub-cells in the form of a rectangular grid that is temporarily overlaid on each computational cell when collisions are to be calculated. The number of divisions in each cell is adapted to the number of simulated molecules in the cell at the time such that there is only one or two molecules in each grid location. The molecules are indexed to this grid in the usual way and the selection process effectively yields nearest-neighbor collisions in a computationally efficient manner.

These transient adaptive sub-cells have been implemented in Version 3 of the DS2G program and have proved to be highly advantageous. Not only is less computation time and memory required for a given mean separation distance of the collision partners, but the new procedures lead to far smaller separation distances than the smallest possible distances with the traditional sub-cells. A further advantage is that the user is not only relieved of the responsibility for choosing the sub-cell size, but there is no longer a need to set different cell and sub cell sizes over complex flowfields. Instead, the smallest possible spacing of the collision partners is automatically achieved in all regions of the flowfield.

In order to check the efficacy of the transient sub-cells in the DS2G program, diagnostic output was added to the TECPLOT file for the flowfield properties. This displayed the ratio of the local mean separation between collision partners to the local mean free path. The ratio of the time step to the local mean collision time was also displayed and this highlighted a problem that has been well known, particularly for hypersonic flows with large variations in density. If the time step is smaller than the mean collision time in the regions of highest density and/or temperature, it is much smaller than the values that are needed in the other regions of the flowfield and the calculation is inefficient. This has led to a tendency to set an excessively high time step. The general guideline is to set the time step such that the number of collisions in the step is about one quarter the number of simulated molecules, but the diagnostic output showed that this is much too large for problems with large variations in density or temperature. Cell-dependent time steps have been successfully employed by some workers, but these lead to problems with efficient programs that do not calculate trajectory intersections with cell boundaries.

(b) Molecule and cell dependent time steps

New procedures have been introduced that make the time step <u>vary with every molecule</u> <u>as well as with every cell</u>. To this end, separate time variables are associated with every molecule and every cell. The procedures keep all these variables concurrent with the overall time variable.

The overall time variable is advanced in very small time steps, but only a small fraction of the molecules are moved and collisions are calculated in only a small fraction of the cells at any one time step. The mean collision time is kept for each cell and collisions in a cell appropriate to a time interval of 0.3×the local mean collision time are calculated whenever the cell time variable falls 0.15×the local mean collision time behind the overall flow time. Similarly, a molecule will generally be moved through 0.3×the mean collision time of its current cell when its time variable falls 0.15×this local mean collision time behind the overall flow time. However, there may be other constraints on the length of the molecule time step based. These include the well-established limit on the time step near the axis when "two-dimensional logic" is employed in axially symmetric calculations. Also, the logic can often be simplified if there is a molecule velocity dependent restriction that limits the distance that a molecule can move in a single step. The step through which the overall time is advanced is kept under 0.15×the minimum mean collision time in any cell. The values of these multiples will be optimized as experience is gained with the new procedures.

Because of the very small overall time step and the small number of cells for which collisions are calculated at each step, the implementation of the traditional indexing routine at each step would involve a prohibitive computational effort. This problem has been solved through the introduction of "bi-directional" indexing. The traditional index array is comprised of the molecule numbers in order of the cells. If the address of the corresponding entry in this array is stored for each molecule, the indexing may be kept up to date continuously as molecules move from cell to cell. The index array must also be extended with sufficient free space between cells to cope with the fluctuations in the number of molecules in individual cells. Some general rearrangement takes place from time to time to allow for particularly large fluctuations or systematic changes in the distribution of molecules. An additional but minor change is that the entering molecule flux must be associated with the cells and the entry of new molecules must occur during the collision routine rather than during the move routine. In many other procedures, the ability to assign different times to molecules leads to a simplification of the program.

These new procedures have been implemented in a "test" version of the DS2G program. The computational speed of the first demonstration case increased by a factor of more than three. This was for a flow with a stream Mach number of two and a realistic hypersonic test case showed a speed gain factor between four and five. Other test cases, such as uniform flows, were calculated and there was no sign of undesirable side effects.

The new procedures are not only more efficient but, because of the automatic setting of the time step, it is no longer possible for this to be incorrectly specified. The transient-adaptive sub-cells effectively prevent the incorrect setting of cell size and a poor calculation can be made only if the total number of simulated molecule is too small. This could cause the mean separation of collision partners to exceed the local free path but, since this is continuously checked, the program can be made to stop if a bad calculation is attempted. These new procedures enable DSMC programs to be made foolproof.

2. The DS3W and DS2A Programs

The introduction of the transient-adaptive sub-cells permits the use of the simplest possible cell structure – a uniform rectangular grid. However, there are difficulties when a thin body causes sections of a single rectangular element to be on the opposite sides of the body. In addition, there are demonstrable advantages at low Knudsen numbers in having surface cells that conform to the geometry. The solution is to wrap cells layers of uniform thickness around all surfaces, with the total depth of this surface cell layer set to be larger than the basic rectangular cell size. This scheme requires the calculation of the distance of a molecule from the surface when it is within the surface cell layer. Fast scaling can then be used to determine the layer within a cell group. Also, for steady flows, it is possible to implement the "DTM-FNUM" scaling that has proved to be very advantageous for entry type calculations.

For three-dimensional flows over surfaces that are defined by triangular elements, surface cell layer groups are defined by their distances above the triangle, above edges that are sufficiently convex to the flow, and above vertices that are sufficiently convex to the flow. Depending on the degree of convexity, the edge-based layer may have to be further divided on the basis of the elevation angle and vertex-based layers may have to be divided in both elevation and azimuth. The solid geometry is not trivial, but expressions have been derived for the definition of all these types of surface defined cells. The junctions between cell groups can be define analytically, but it is computationally more efficient to allow some degree of ambiguity and, when more than one cell is valid, the closest one is chosen.

This geometry scheme is being implemented in a program DS3W for the flow past three-dimensional bodies. The program is in structured FORTAN 90 and is being written such that it can be progressively debugged, subroutine by subroutine, while it is being written. While the geometry and cell definition routines have been completed, the introduction of the variable time step procedures has created an urgent need for a new general program for two-dimensional and axially symmetric flows. Work on DS3W has therefore been suspended until program DS2A has been completed.

Program DS2A employs the two-dimensional version of the geometry in program DS3W, but is more general in that there can be multiple surfaces. It can therefore be applied to internal as well as external flows. The user will specify the geometry, the flow conditions and the number of megabytes of memory that are available. The computational parameters will be set automatically and, if the available memory does not allow a sufficient number of simulated molecules for a good calculation, the program will stop with an appropriate warning. To date, the geometry and cell definition subroutines have been completed for this program also.

3. Papers Presented

The following conference papers were presented during this period:
Knudsen and Mach Number Effects on the Development of Wake Instabilities, AIAA 36th Aerospace Sciences Meeting, Reno, January 1998.
Physics by Default – the Art of Phenomenological Modeling, 5th International Symposium on the Mathematical Aspects of Fluid and Plasma Dynamics, Maui, June 1998.
Shock Wave Structure in a Gas with Transverse Gradients, 21st International Symposium on Rarefied Gas Dynamics, Marseille, July 1998.

4. Miscellaneous Applications and Program Modifications

Check calculations for Mars entry flows indicated that the procedures in the DS2G program for vibrational relaxation rates were less than satisfactory for carbon dioxide. The variable relaxation rates had been linked to the macroscopic temperatures in the cells. This was satisfactory with gases such as nitrogen and oxygen, but in the case of carbon dioxide the large number of internal degrees of freedom produced much larger differences between the translational and overall temperatures. This led to anomalous relaxation rates and the procedures were modified to make all relaxation processes dependent on the energy in the individual collisions. This was a reversion to earlier procedures in which dependence on macroscopic temperatures had been avoided on the grounds that it was physically unrealistic. The vibrational relaxation behavior of carbon dioxide was then consistent with expectations.

The transient sub-cells in the general program DS2G made it possible for this program to deal with unsteady flows without resort to ensemble averaging. The necessary changes to the sampling procedures were incorporated into version 3.1. A number of CFD and DSMC studies have recently been made of hypersonic biconic flows that include an extensive region of separated flow. While these studies have assumed steady flow, the flow conditions bordered on those at which unsteady flow would be expected. The unsteady DS2G calculations have shown that the unsteady flow development phase is more protracted than had been thought and may involve secondary vortices and some oscillation of the shock location. The 25°-65° biconic, $M=10$ test case is currently being calculated by Version 3.1 of DS2G at a Reynolds number approaching 50,000. The single-vortex separated region that was characteristic of the lower Reynolds number cases has been replaced by a multi-vortex system with the first secondary vortex appearing on the 25° surface well upstream of the corner. This calculation on a 450 MHz Pentium II system with 512 Mb memory will last 10 weeks. The introduction of the new DS2A program is expected to cut the execution time for this type of flow by a factor of ten. It should then be possible to extend these calculations into the regime where the separated region becomes permanently chaotic, although the assumption of axially symmetric flow would then be dubious.

The demonstration of a transition to a permanently chaotic state in axially symmetric Taylor-Couette flow has been the most important result from the flow studies under this series of subcontracts. Stefanov, Roussinov, Cercignani, Giurin and Struckmeier have recently shown (21st RGD Symposium, Marseille, 1998) that a similar transition occurs in two-dimensional Rayleigh-Benard flows. Both DSMC and Navier-Stokes solvers were employed in this study and a similar transition to a permanently chaotic state occurred for both the particle and continuum approaches. They characterized this behavior as a "strange attractor" and state unequivocally that it represents the first stage of the transition to turbulence in the flow. To be physically meaningful, transition calculations must be three-dimensional. The N-S and DSMC computations were of similar magnitude in this case but, since N-S calculations do not scale linearly with the number of grid points, DSMC could well be faster when three-dimensional calculations are made. Also, because the ratio of the minimum vortex size to the mean free path is expected to be inversely proportional to the Mach number, the Navier-Stokes equations may not be valid for transition in the case of hypersonic flow. It will be ten to fifteen years before three-dimensional DSMC studies of the initiation of turbulence become possible on personal computers. These calculations are possible on the largest of the contemporary parallel machines, but the very long runs that would be required would probably not be cost effective. The calculations will become feasible within the next few years.

AIAA 98-2939

Solution of Transitional Wake Flows at Mach 10

Robert P. Nance
North Carolina State University, Raleigh, NC

Brian R. Hollis and Thomas J. Horvath
NASA Langley Research Center, Hampton, VA

H. A. Hassan
North Carolina State University, Raleigh, NC

**7th AIAA/ASME Joint Thermophysics Conference
June 15–18, 1998/Albuquerque, NM**

Solution of Transitional Wake Flows at Mach 10

Robert P. Nance[*]
North Carolina State University, Raleigh, NC

Brian R. Hollis[†] and Thomas J. Horvath[†]
NASA Langley Research Center, Hampton, VA

H. A. Hassan[‡]
North Carolina State University, Raleigh, NC

Modeling enhancements are investigated for transition and turbulence in hypersonic blunt-body flows. The current approach combines the k-ζ (Enstrophy) compressible turbulence model with a new transition mechanism appropriate for free shear layers, such as those encountered in blunt-body wakes. Prediction of transition onset is provided by a minimum shear-stress criterion applied along the sting. This method is applied to several perfect-gas Mach 10 flows over 70-deg blunted cones. Improved prediction of the peak sting heating rates is indicated when compared to results obtained using streamwise instability modes. Grid refinement is also investigated, and is found to provide additional improvement in the agreement between the present approach and experimental data. The favorable comparisons are a further indication that transition to turbulence is indeed present in the blunt-body wake flows examined.

Nomenclature

k	Turbulent kinetic energy
p	Pressure
$\overline{Q}$	Reynolds- or time-averaged value of Q
$\tilde{Q}$	Favre-averaged value of Q
q	Heat-transfer rate
R_n	Nose radius
Re	Reynolds number
s	Linear surface distance
T	Temperature
U	Velocity magnitude
u_i	Velocity vector
$\bar{x}$	Distance measured along sting support
δ	Boundary- or shear-layer thickness; k-ζ model constant
δ^*	Boundary-layer displacement thickness
δ_{ij}	Kronecker delta
Γ	Intermittency
λ	Transition-extent parameter
μ	Dynamic viscosity
ν	Kinematic viscosity
ρ	Density
τ	Characteristic time scale
τ_{ij}	Reynolds stress tensor
ω	Transitional frequency
ω_i	Vorticity vector
ζ	Enstrophy

Subscripts

1	Value at edge of shear layer
D	Value based on cone diameter
e	Value at edge of boundary layer
T	Total value
t	Turbulent value
tr	Transitional value
∞	Freestream

Superscripts

l	Laminar (non-turbulent) value
t	Turbulent value
$*$	Dimensional transitional quantity

[*]Research Assistant, Department of Mechanical and Aerospace Engineering, Student Member AIAA.

[†]Aerospace Technologist, Aerothermodynamics Branch, Aerodynamics and Gas Dynamics Division, Member AIAA.

[‡]Professor, Department of Mechanical and Aerospace Engineering, Associate Fellow AIAA.

Introduction

Current and proposed planetary exploration missions, such as the recent Mars Pathfinder project, have spurred renewed interest in the physics of blunt-body wake flowfields. Accurate characterization of the near-wake environment is important for the design of entry configurations, since the nature of the wake closure typically places constraints on payload size and location. Recent activity in this discipline has included a number of experiments on blunt-cone models, such as the work carried out by several teams of researchers[1-4] in support of AGARD Working Group 18. These WG 18 tests have been conducted in several hypervelocity facilities with the objective of characterizing the fluid dynamic phenomena present in the wake region
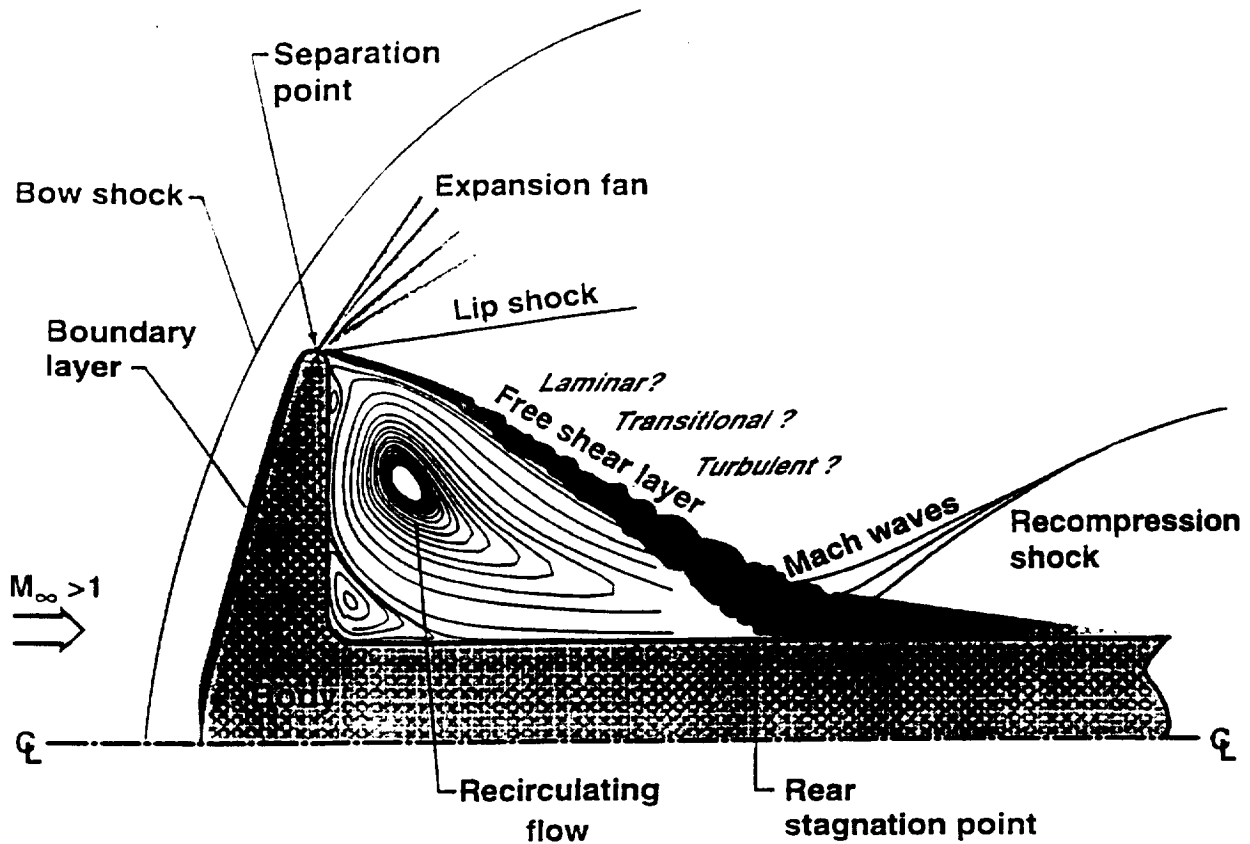
Fig. 1   Schematic of hypersonic blunt-body wake flow

for flows exhibiting real-gas behavior (Fig. 1). The tests were conducted at nominally identical test conditions to help assess and quantify facility-to-facility performance. Initial comparisons of measurement with prediction indicated that the measured peak heating rates along the model sting support were two to three times greater than those predicted by laminar Navier-Stokes computations. A variety of explanations were proposed (such as flow establishment, real-gas phenomena, and wake rarefaction) to explain this disparity. Subsequent perfect-gas tests performed by Horvath and coworkers[5,6] on the AGARD WG 18 geometry, as well as studies by Hollis and Perkins[7] using a similar configuration, suggested instead that wake shear layer transition was responsible for the higher-than-anticipated heating levels at reattachment.

Accurate predictions of such high-speed transitional flows are important for the design of hypersonic vehicles. However, there has been little effort to date towards development of computational tools capable of predicting transitional and turbulent flow in blunt-body wakes.

Previous efforts by Nance, Horvath and Hassan[8] to predict transitional blunt-body flow at a freestream Mach number of 6 yielded improved agreement with experimental heat-flux data obtained by Horvath, McGinley and Hannemann.[5] In the present work, we

use the same general approach as in Ref. 8, but the mechanism responsible for transition is different. The earlier work utilized streamwise instabilities, namely Tollmien-Schlichting and Mack modes. Currently, however, we consider transition as a result of free-shear-layer instability. Two configurations shall be considered here, both of which were tested in the 31" Mach 10 Air Tunnel at NASA Langley Research Center. These geometries, shown in Figures 2 and 3, correspond to those tested by Horvath and Hannemann[6] and Hollis and Perkins,[7] respectively.

Modeling Approach

This work is based on solution of the Favre-averaged Navier-Stokes equations in conjunction with a two-equation model modified for use in transitional flow-fields. In this context, we seek to determine the influence of the transitional or turbulent fluctuations on the mean flow variables, instead of predicting the fluctuations themselves. Closure is obtained by specifying equations for the modeled variables, as well as expressions for disturbance-related quantities in the non-turbulent portions of the flow.

Transport Equations for Modeled Quantities

Fluctuation velocity and time scales are provided in this work by the compressible k-ζ model first proposed by Robinson, Harris and Hassan.[9] This approach is

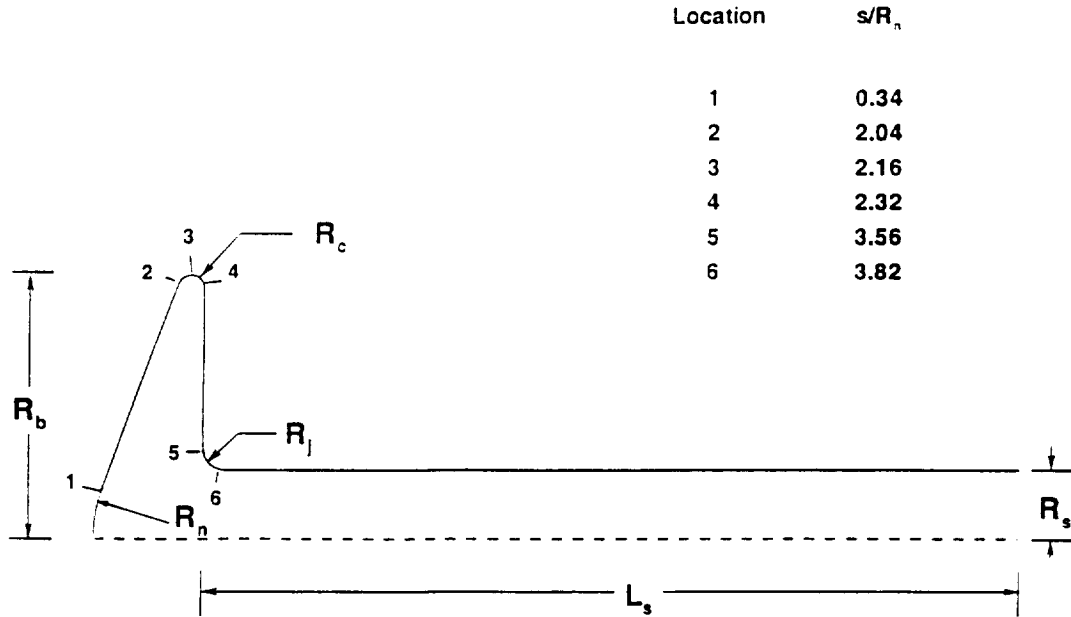| Location	s/R_n
1	0.34
2	2.04
3	2.16
4	2.32
5	3.56
6	3.82

Fig. 2 70-deg blunt cone and sting geometry employed by Horvath and Hannemann

very similar as that used in Ref. 8, with minor modifications to some of the terms and constants appearing in the model. The k-ζ equation set used in this work is listed below, and model constants are listed in Table 1.

$$\bar{\rho}\frac{Dk}{Dt} = \tau_{ij}\frac{\partial \bar{u}_i}{\partial x_j} + \frac{\partial}{\partial x_j}\left[\left(\frac{\mu}{3} + \frac{\mu_T}{\sigma_k}\right)\frac{\partial k}{\partial x_j}\right]$$
$$- C_1\frac{\bar{\rho}k}{\tau_\rho} - \frac{\bar{\rho}k}{\tau_k} - \frac{1}{C_k}\frac{\overline{\nu_T}}{\bar{\rho}}\frac{\partial\bar{p}}{\partial x_k}\frac{\partial\bar{p}}{\partial x_k} \qquad (1)$$

$$\bar{\rho}\frac{D\zeta}{Dt} = \frac{\mu_T}{\sigma_r}\frac{\partial \bar{\omega}_i}{\partial x_j}\left[\left(\frac{\partial \bar{\omega}_i}{\partial x_j} + \frac{\partial \bar{\omega}_j}{\partial x_i}\right)\right]$$
$$+ \frac{\partial}{\partial x_j}\left[\left(\mu + \frac{\mu_T}{\sigma_\zeta}\right)\frac{\partial\zeta}{\partial x_j}\right] - \frac{\beta_5}{\sqrt{R_t} + \delta}\bar{\rho}\zeta^{\frac{3}{2}}$$
$$+ \left(\alpha_3 b_{ij} + \frac{2}{3}\delta_{ij}\right)\bar{\rho}\zeta\bar{s}_{ij} - \frac{\beta_4\zeta\tau_{ij}\bar{\omega}_i\bar{\omega}_j}{k\bar{\omega}}$$
$$- \frac{2\beta_6\tau_{ij}\nu_T}{k\nu}\bar{\omega}\bar{\omega}_i\bar{\omega}_j + \frac{\beta_7\bar{\rho}\zeta}{\bar{\omega}^2}\bar{\omega}_i\bar{\omega}_j\bar{s}_{ij}$$
$$+ \max(P_\zeta, 0) - \frac{C_{\zeta_1}\mu_T\zeta\bar{\omega}}{k\tau_\rho} - 2\bar{\rho}\zeta\bar{s}_{kk} \qquad (2)$$

where

$$\tau_{ij} = \mu_T\left(2\bar{s}_{ij} - \frac{2}{3}\delta_{ij}\bar{s}_{kk}\right) - \frac{2}{3}\delta_{ij}\bar{\rho}k$$

$$b_{ij} = \frac{\tau_{ij} + \frac{2}{3}\bar{\rho}k\delta_{ij}}{\bar{\rho}k}$$

$$s_{ij} = \frac{1}{2}\left(\frac{\partial \bar{u}_i}{\partial x_j} + \frac{\partial \bar{u}_j}{\partial x_i}\right)$$

$$k = \frac{1}{2}\widetilde{u_k''u_k''} \quad ; \quad \zeta = \widetilde{\omega_k''\omega_k''}$$

$$R_t = \frac{k^2}{\nu^2\zeta} \quad ; \quad \nu_T = \frac{\mu_T}{\bar{\rho}}$$

$$P_\zeta = \bar{\rho}\frac{D\bar{p}}{Dt}\frac{k\bar{\omega}}{\nu\bar{p}\sigma_p}\frac{1}{(1+\delta_\rho)}$$

$$\delta_\rho = \frac{\sigma_\rho}{\bar{p}}\sqrt{\frac{2kR_t}{\zeta}\left(\frac{\partial\bar{p}}{\partial x_k}\right)^2}$$

$$\frac{1}{\tau_\rho} = \frac{1}{\bar{p}}\sqrt{k(\partial\bar{p}/\partial x_k)^2}$$

Specific alterations to the k-ζ equation set include reformulation of the density-gradient timescale and reduction of the pressure-work constant C_k. These modifications were made to preserve Galilean invariance while maintaining good agreement with experimental data when applied to transonic airfoils. Note that the Reynolds stress tensor is modeled using the Boussinesq approximation. Preliminary investigations of these flowfields employing a partial differential stress model, wherein the Reynolds normal stresses are predicted using model transport equations, yielded no improvement in predictions when compared to the Boussinesq approach.
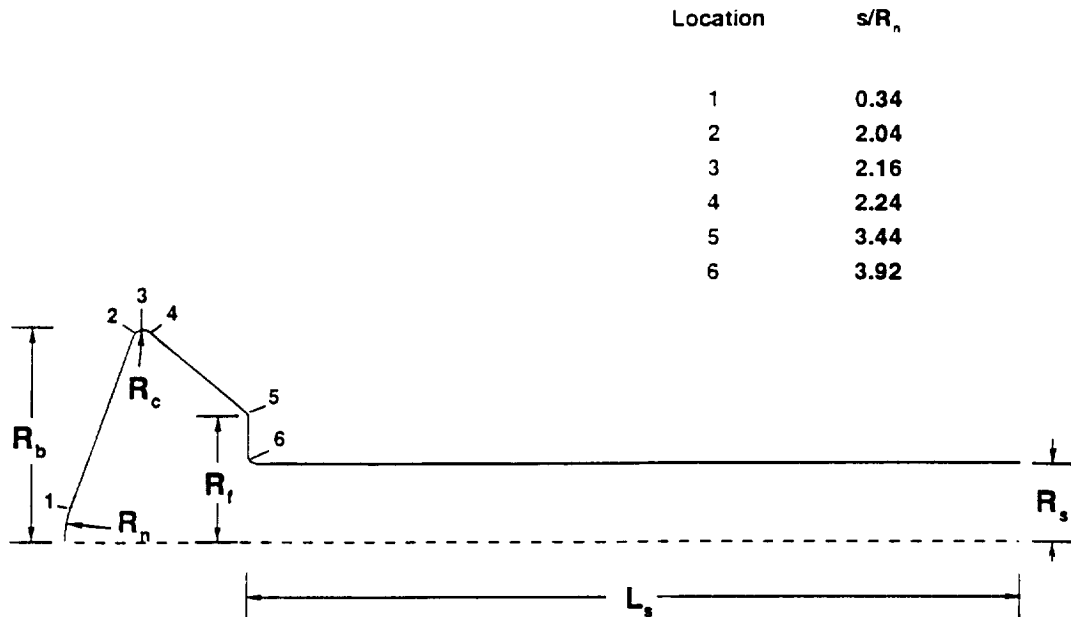
Location	s/R$_n$
1	0.34
2	2.04
3	2.16
4	2.24
5	3.44
6	3.92

Fig. 3   70-deg blunt cone and sting geometry employed by Hollis and Perkins

Table 1 k-ζ model constants

Constant	Value
C_μ	0.09
α_3	0.35
β_4	0.42
β_5	2.37
β_6	0.10
β_7	1.50
σ_p	0.065
σ_r	0.07
σ_ρ	65.0
$1/\sigma_k$	1.80
$1/\sigma_\zeta$	1.46
δ	0.10
C_1	0.60
C_k	1.00
C_{ζ_1}	2.10

Instability Mechanism

An advantage of the k-ζ formulation is that the model terms are derived without explicitly declaring the nature of the fluctuation. Hence, the model may be used to predict the entire flowfield, including transitional and fully turbulent regions, provided an appropriate stress-strain relation is employed. Such a relationship is obtained in part by defining the total eddy viscosity in terms of a fully turbulent contribution and a contribution due to non-turbulent fluctuations:

$$\mu_T = (1 - \Gamma)\mu_{tr} + \Gamma\mu_t \tag{3}$$

Eq. 3 can be rewritten as a combination of terms of non-turbulent and fully turbulent timescales as follows:

$$\mu_T = C_\mu \bar{\rho} k \tau_\mu \tag{4}$$

$$\tau_\mu = (1 - \Gamma)\tau_\mu^l + \Gamma\tau_\mu^t \tag{5}$$

where the fully turbulent timescale is given as

$$\tau_\mu^t = \frac{k}{\nu\zeta} \tag{6}$$

and the non-turbulent timescale is dictated by the mechanism responsible for transition. In Ref. 8, non-turbulent disturbances were considered through a model accounting for Mack's[10] first and second modes. Hence, the non-turbulent characteristic timescale was originally defined as

$$\tau_\mu^l = \tau_1 + \tau_2 \tag{7}$$

where the two timescales are defined in terms of first- and second-mode characteristic frequencies, and the frequencies are correlated as
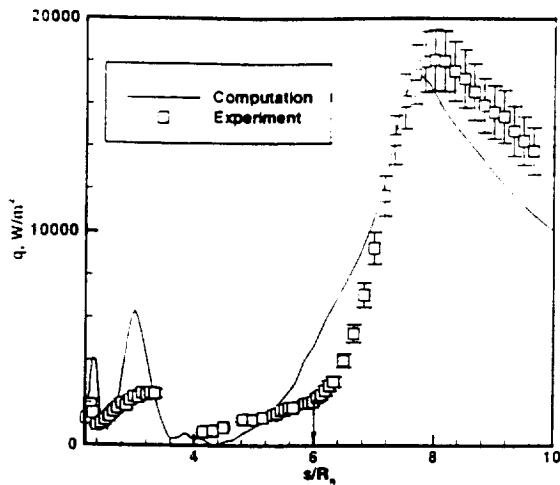
Fig. 4 Base plane and sting heating results obtained using earlier model–Mach 6, $Re_D = 2 \times 10^6$

Fig. 5 Base plane and sting heating results obtained using earlier model–Mach 10, $Re_D = 1 \times 10^6$

$$\tau_1 = \frac{a}{\omega_{TS}} \quad ; \quad \tau_2 = \frac{b}{\omega_{SM}} \tag{8}$$

$$\frac{\omega_{TS}\nu}{U_e^2} = 3.2 Re_\delta^{-3/2} \tag{9}$$

$$\omega_{SM} = \frac{U_p}{2\delta} \approx \frac{U_p}{M_e^2}\sqrt{\frac{Re_e}{s}} \tag{10}$$

where U_p, the phase velocity, is taken to be 0.94 times the edge velocity U_e. As illustrated in Ref. 8, this mechanism yielded good agreement between computation and the experimental heating data[5] for a representative Mach 6 case, also using the AGARD WG 18 geometry. Freestream conditions for the Mach 6 cases discussed here are listed in Table 2. The Mach 6 result

Table 2 Freestream conditions for representative Mach 6 cases

Re_D	ρ_∞, kg/m^3	U_∞, m/s	T_∞, K
2×10^6	6.45×10^{-2}	943.8	62.7
0.5×10^6	1.68×10^{-2}	931	63.3

shown in Fig. 4, which was obtained using the original instability model, demonstrates that this approach is capable of providing reasonable predictions of the location and magnitude of the peak heat-transfer rate along the sting for this case. The vertical arrow in the figure denotes the location of transition onset predicted by the computation. When this model is applied to representative Mach 10 flowfields, however, the agreement is considerably poorer, as illustrated in Figures 5 and 6. The degradation of agreement with increasing Mach and decreasing Reynolds number is a sign of an improperly modeled transition process.

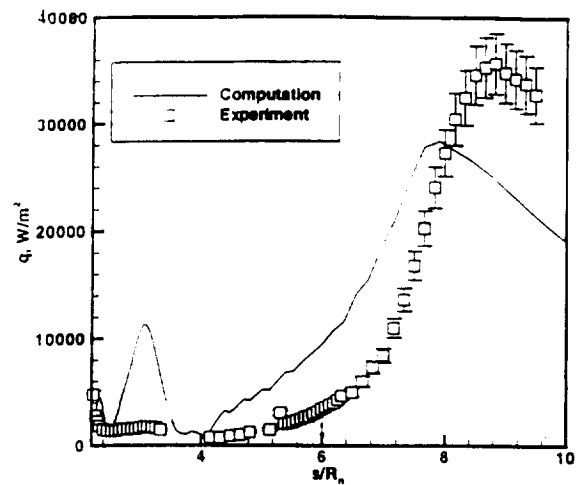A correct transition mechanism should yield good results for both Mach 6 and Mach 10 experiments over
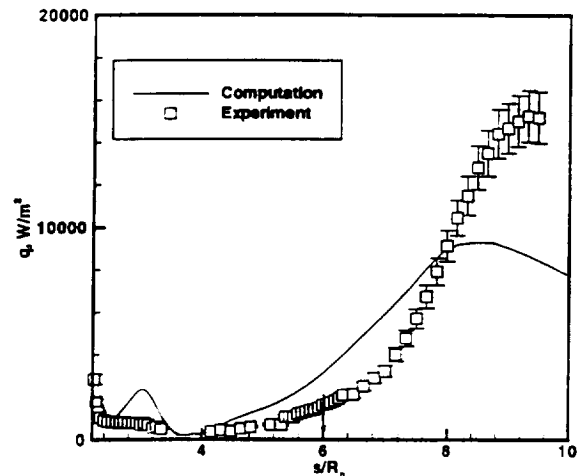

Fig. 6 Base plane and sting heating results obtained using earlier model–Mach 10, $Re_D = 2.8 \times 10^5$

a range of Reynolds numbers. Because the mechanism used in Ref. 8 was inadequate for the Mach 10 flowfields, the new model focuses instead on transition in the free shear layer emanating from the shoulder of the cone, shown in Fig. 1. Such free shear layers are always unstable. The most amplified frequency, which is required for the present formulation, is obtained from linear stability theory predictions for compressible mixing layers.[11] For all the Reynolds numbers, Mach numbers, and and velocity ratios considered in Ref. 11, the nondimensional value of the most amplified frequency was found to be relatively invariant, always falling in the range $\omega = 0.05$ to $\omega = 0.15$. This nondimensional frequency is related to the dimensional value by

Table 3 Freestream conditions and grid dimensions for Mach 10 cases

Case	Geometry	Re_D	$\rho_\infty, kg/m^3$	$U_\infty, m/s$	T_∞, K	Grid 1	Grid 2
1	Horvath and Hannemann	1×10^6	1.613×10^{-2}	1426	51.27	189×75	377×149
2	Horvath and Hannemann	2.80×10^5	4.471×10^{-3}	1415	53.15	189×75	377×149
3	Hollis and Perkins	3.15×10^5	1.646×10^{-2}	1425	51.48	125×90	249×179
4	Hollis and Perkins	8.23×10^4	4.51×10^{-3}	1416	53.31	125×90	249×179

$$\omega^* = \omega U_1^* / \delta^* \qquad (11)$$

where U_1 is the velocity of the higher-velocity stream, and δ^* is proportional to the thickness of the mixing layer:

$$\delta^* = \sqrt{\mu_1^* \bar{x}^* / \rho_1^* U_1^*} \qquad (12)$$

In the above, $\bar{x}^*$ represents the dimensional distance from the start of the mixing layer, which in this case is taken to correspond to distance along the sting support. The dimensional frequency can be used to define the non-turbulent characteristic timescale:

$$\tau_\mu^l = \frac{d}{\omega^*} \qquad (13)$$

For the present work, the nondimensional frequency appearing in Eq. 11 is taken as 0.10, and the model constant d is chosen as 5.0.

The dissipation term in the k equation is also modified to account for transitional effects by computing the representative decay time for turbulent kinetic energy as

$$\frac{1}{\tau_k} = \frac{1 - \Gamma}{\tau_k^l} + \frac{\Gamma}{\tau_k^t} \qquad (14)$$

where

$$\frac{1}{\tau_k^l} = C \frac{\nu_T}{\nu} \bar{s} \quad ; \quad \tau_k^t = \tau_\mu^l$$

$$\bar{s}^2 = \bar{s}_{ij} \bar{s}_{ij}$$

and the model constant C is chosen as 0.01. While a more rigorous approach would correlate ω with parameters such as Mach number and Reynolds number, there is insufficient data for performing such a correlation at present. The values listed above were calibrated through application to the Mach 6, $Re_D = 2 \times 10^6$ blunt-body flow previously considered in Ref. 8.

Transition Prediction and Intermittency Calculation

As in Ref. 8, we choose the transition onset location as the location of minimum shear stress along the sting. The minimum heat-flux criterion proposed earlier is not considered here, since it was found to yield poorer agreement with available data. A criterion based on location of flow reattachment along the sting was also considered, but was discarded because it also yielded degraded comparisons.

The intermittency correlation due to Dhawan and Narasimha[12] is retained from the previous work:

$$\Gamma = 1 - \exp\left(-0.412\xi^2\right) \qquad (15)$$

However, the intermittency determination in Ref. 8 utilized a distance parameter ξ based on linear surface distance starting from the forward stagnation point. In keeping with the notion of shear-layer instability, the parameter ξ is now based on distance along the sting. That is,

$$\xi = \frac{\max\left(\bar{x} - \bar{x}_t, 0\right)}{\lambda} \qquad (16)$$

where
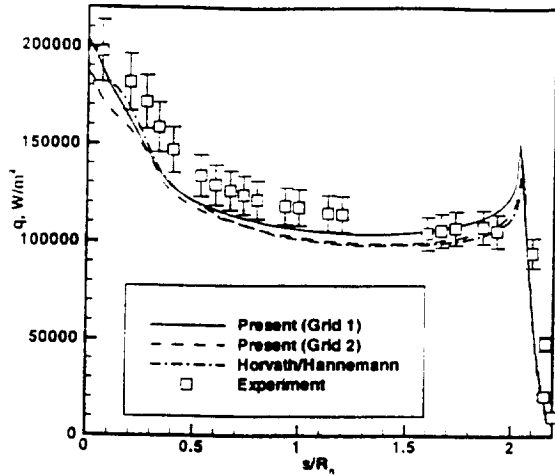
$$Re_\lambda = 9.0 Re_{\bar{x}_t}^{0.75} \qquad (17)$$

and the Reynolds numbers appearing above are based on conditions at the edge of the layer. In Eq. 16, $\bar{x}_t$ is the location of transition onset, and is determined as part of the solution to correspond to the location of minimum skin friction along the sting.
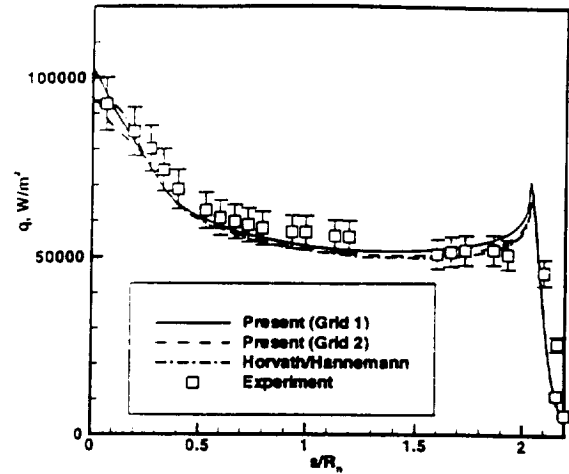
Numerical Method

The modeling proposed here has been incorporated into Olynick's[13] two-dimensional/axisymmetric implicit solver for hypersonic flows. This algorithm solves the governing equations for 5-species air in thermochemical nonequilibrium. The solver uses Roe's flux-difference splitting[14] for the inviscid flux, extended to higher order using MUSCL variable extrapolation[15] with a minmod slope limiter. Time integration is accomplished using the diagonal implicit variant of Yoon and Jameson's Lower-Upper Symmetric Gauss-Seidel method,[16] which only requires the inversion of diagonal matrices. This property is attractive for nonequilibrium flows, where a large number of partial differential equations must be solved.

Since the current flowfields under investigation are perfect-gas, vibrational relaxation and chemical reactions are disabled to obtain the results in this study. Additionally, the high-temperature transport-property calculations originally used in the code were replaced with Sutherland's law for viscosity and a constant laminar Prandtl number of 0.72. Closure for the Favre-averaged energy equation is accomplished using a constant turbulent Prandtl number of 0.89.
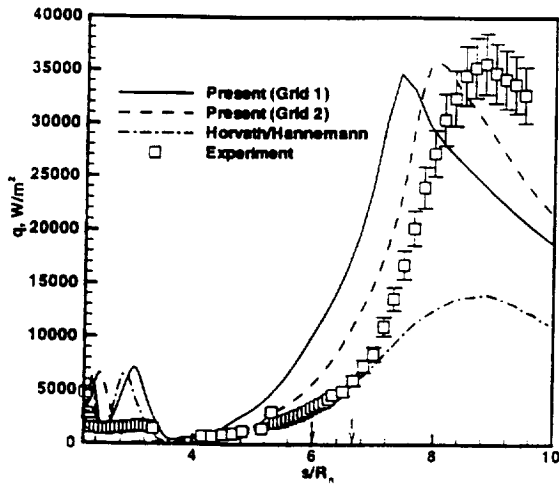
To promote physically realizable solutions, the computed values of k and ζ are required to remain positive throughout the computational domain. How-
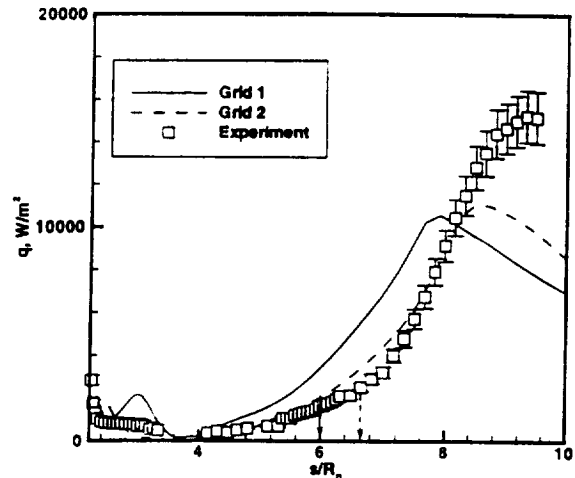
a) Forebody and shoulder

a) Forebody and shoulder

b) Base plane and sting

Fig. 7   Influence of grid refinement for case 1–Mach 10, $Re_D = 1 \times 10^6$

b) Base plane and sting

Fig. 8   Influence of grid refinement for case 2–Mach 10, $Re_D = 2.8 \times 10^6$

ever, no artificial limitation on turbulent kinetic energy production was imposed in the numerical method. Transitional solutions are started by running the solver in a laminar-flow mode for about 100 iterations.

Results

As mentioned earlier, two blunt-cone configurations were considered in this study. Two flow conditions are examined for each geometry, for a total of four cases. In addition, some Mach 6 conditions were revisited. The freestream Reynolds numbers for each case, as well as dimensional freestream conditions, are listed in Table 3. Since no data are available regarding the freestream disturbance conditions in the Langley 31" Mach 10 facility, a freestream turbulence intensity of 0.9% was assumed for all four of the Mach 10 cases.

Additionally, the wall temperature in each solution is fixed at 300 K. Table 3 also lists the dimensions of the two grids used for each condition.

Grid Refinement Study

We shall begin by examining the influence of grid resolution on the heating predictions for each of the four cases. In each case, the results shown are obtained using the newly developed instability mechanism described above. Fig. 7 shows heating results for the first of the four cases, with separate graphs for the forebody/shoulder heating distribution and the base plane/sting heating distribution. The results are separated in this manner because of the large differences in forebody and base plane heating magnitudes. As shown in Fig. 7(a), both the coarse-grid and fine-grid

.ieat-transfer predictions agree fairly well with the experimental data. This plot also demonstrates that the present forebody results agree well with the laminar solution performed by Horvath and Hannemann.[5] The grid employed in Ref. 6 was 771 × 301. Hence, it appears that the current forebody result obtained using grid 2 is well-resolved. Furthermore, the forebody heating results support the notion that transition to turbulence does not take place on the forebody.

Fig. 7(b) compares the present results on coarse and fine grids along the back plane and sting. A laminar-flow heating result for this condition[6] is also shown in this plot. This result demonstrates the extent to which laminar calculations underpredict the measured heat flux along the sting. Such behavior is typical of all the laminar solutions presented in References 5, 6, and 7. Therefore, comparisons with laminar-flow predictions along the base and sting will not be shown in the remaining figures.

It is clear that increased grid refinement has a distinct effect on the sting heat-transfer distributions obtained using the present approach. This trend is similar to that previously observed in laminar computations for these flows.[5-7] While the magnitude of the peak heat flux does not change greatly, the location of the peak heating is visibly shifted downstream. This movement arises because the fine-grid solution predicts a slightly larger recirculation zone; hence, the reattachment point and location of shear-layer impingement are moved downstream. A further consequence of this behavior is that the predicted onset of transition (denoted by the vertical arrows along the horizontal axis) is also moved further downstream. This plot also shows that increased grid refinement tends to improve the agreement between the computation and experimental measurements for this case.

A comparison of the coarse-grid and fine-grid results for the second case is shown in Fig. 8. As in the previous case, the forebody heating distribution compares well with experimental data and previous laminar computations. The sting heating results (Fig. 8(b)) show similar trends to the first case, in that the refined-grid solution predicts a peak heating located farther down the sting. In this case, though, the peak heating magnitude is not as well-predicted as in the first case; the discrepancy between the fine-grid heat flux and the experimental data is still roughly 30%. It is not immediately clear why the agreement for this case is not as good as that seen in the other solutions.

For the third case, Fig. 9 shows that the comparisons are fairly good for both the forebody and sting heating predictions on the fine grid. with the predicted forebody results within or slightly outside of the experimental error bounds. Note that the grid used by Hollis and Perkins[7] for cases 3 and 4 was a 125 × 357 grid. The good agreement between the fine-grid results obtained here and the laminar solutions of Hollis
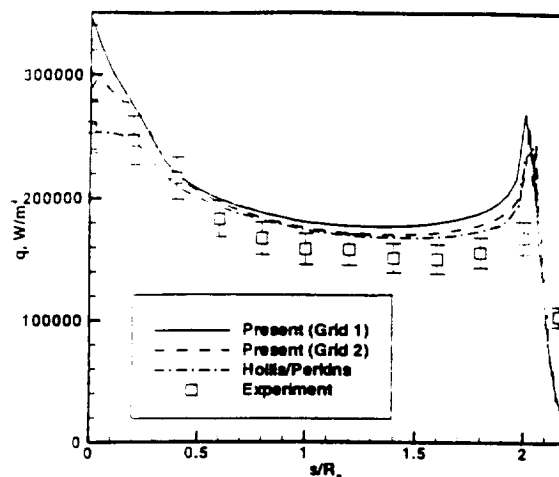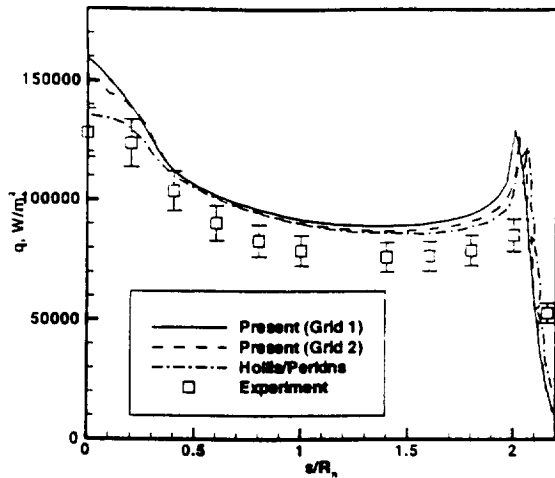

a) Forebody and shoulder
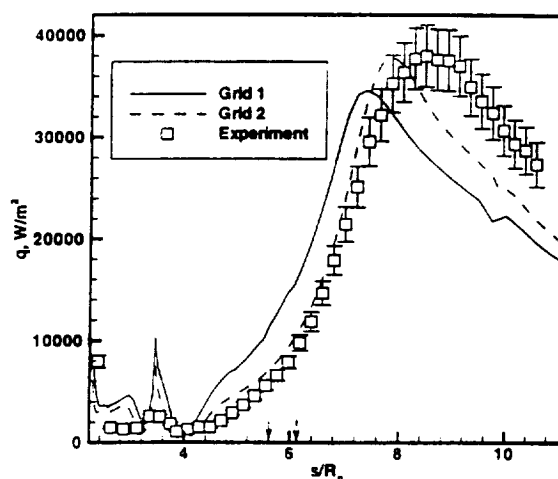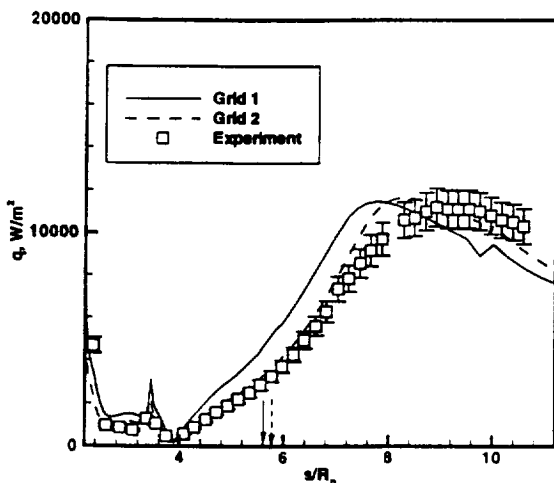

b) Base plane and sting

Fig. 9   Influence of grid refinement for case 3—Mach 10, $Re_D = 3.15 \times 10^5$

and Perkins indicates grid convergence on the forebody for these cases, as well. Along the sting (Fig. 9(b)), we again see that increased grid refinement yields a later heating peak, as well as delayed onset of transition. The refined-grid result also predicts a slightly higher peak heat-transfer rate. As a consequence, most of the features of the sting heating distribution are quite well-predicted, including the initial rise in heat flux corresponding to shear-layer impingement. The anomalous "kinks" in the heating distributions for this and the next case are consequences of a discontinuous slope in the streamwise gridlines, and should not be confused with convergence problems.

The trends in case 4 are similar to those observed in the previous cases. As Fig. 10(a) demonstrates,

a) Forebody and shoulder

b) Base plane and sting

Fig. 10 Influence of grid refinement for case 4—Mach 10, $Re_D = 8.23 \times 10^4$

agreement on the forebody is again quite good. Agreement along the sting is also good; the fine-grid solution shown in Fig. 10(b) compares well, in terms of both magnitude and location, with the measured peak heating rate along the sting support. Once again, the coarse-grid solution predicts the peak heating levels fairly well, but produces a peak heating location visibly upstream of that seen in the data.

Based on the trends seen in these results, as well as the trends in other researchers' laminar computations, further grid refinement would most likely push the peak-heating locations slightly further back on the sting without greatly altering the magnitudes of those peaks.

Comparison to Original Transition Model

The next two figures compare representative coarse-grid results obtained using the new instability mechanism to solutions using the earlier approach. While the results previously presented clearly illustrate the impact of grid refinement on the wake solution, comparison of coarse-grid results is still useful, since grid refinement does not appear to yield very large changes in the magnitudes of the predicted peak heating rates.

Fig. 11 compares sting heating results obtained using the old and new instability mechanisms. It is clear from this graph that the new mechanism provides a greater heating augmentation, and hence better agreement with the data.

Comparisons between the old and new approaches for the third case are shown in Fig. 12. It should be pointed out that the solution using the earlier instability mechanism was actually obtained on a grid with greater normal resolution. In light of the grid-refinement study results presented earlier, though, comparisons between these two results may still be useful. The plot demonstrates again that the new mechanism provides substantially greater peak heating along the sting support, resulting in improved agreement with the experimental data.

While these results indicate that the new instability model performs better for the Mach 10 cases examined in this work, it is reasonable to ask whether it also performs well for other Mach numbers. The new mechanism was calibrated using the data from the earlier Mach 6 case at a freestream Reynolds number of 2×10^6, so good agreement for this condition should be expected. However, comparison of the models at other conditions is certainly worthwhile. The next plot, Fig. 13, compares the two mechanisms for another of the Mach 6 flowfields of Horvath et al.[5] at a freestream Reynolds number of approximately 0.5×10^6 (dimensional conditions listed in Table 2). Again, the 189×75 grid is used for both solutions. This graph demonstrates that the new model yields improved heating predictions for this case as well.

The results shown in Figures 11 through 13 are believed to be sufficient to demonstrate the improvements obtained with the new mechanism. It is interesting to note that, in all but one of these comparisons, the predicted location of transition onset (which corresponds to the location of minimum skin friction) was the same for both models. Increases in grid refinement clearly have a much stronger impact on the location of onset than details of the instability mechanism for the cases considered here.

Concluding Remarks

The combination of transition and turbulence models used in this work was shown to provide improved agreement between the numerical heat-transfer predictions and available experimental data for the Mach
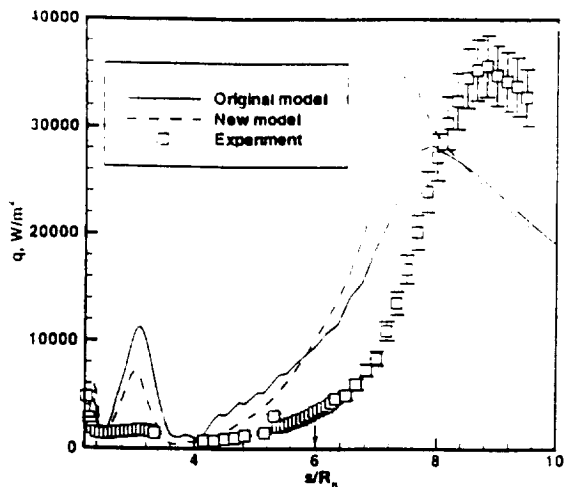
Fig. 11 Comparison of earlier and current approaches for case 1–Mach 10, $Re_D = 1 \times 10^6$ (coarse-grid solutions)
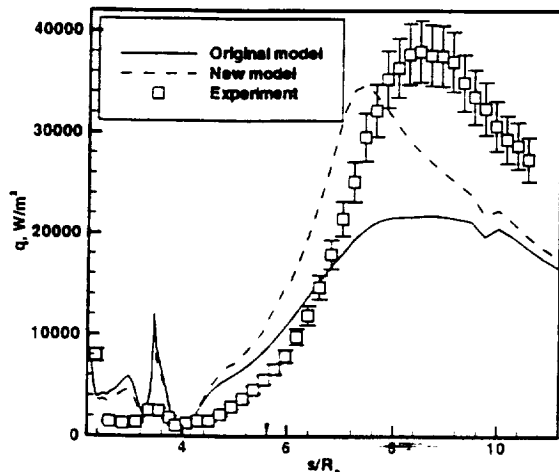

Fig. 12 Comparison of earlier and current approaches for case 3–Mach 10, $Re_D = 3.15 \times 10^5$ (coarse-grid solutions)

10 cases considered. In general, the present method yielded good comparisons to the experimental sting heating data for a wide range of freestream Reynolds numbers.

Coarse-grid solutions produced good predictions of the magnitude of the peak sting heating rates, although the locations of these peaks were consistently predicted upstream of the peaks observed in the measurements. Increasing grid resolution, however, tended to improve the agreement even more by shifting the predicted peak locations further downstream.

The overall agreement between computation and data for the transitional-flow approach described herein is much better than that seen in laminar com-
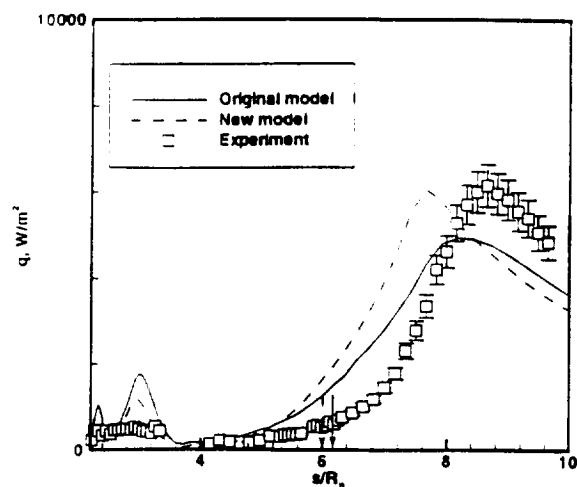

Fig. 13 Comparison of earlier and current approaches for Mach 6 case, $Re_D = 0.5 \times 10^6$ (coarse-grid solutions)

putations for the same flow conditions. This improvement lends further support to the notion that transition to turbulence does occur in the blunt-body flows examined in this study.

The results presented here indicate that treating transition in a turbulence-like manner is a viable approach for studying transitional/turbulent high-speed flows. Moreover, it illustrates the importance of employing the correct transition mechanism in formulating the closure model. Thus, although stability codes did not play a direct role in the present calculations, linear stability theory results were very important in developing the present instability mechanism.

Acknowledgments

References

[1] Holden, M., Kolly, J., and Chadwick, K., "Calibration, Validation and Evaluation Studies in the LENS Facility," AIAA Paper 95-0291, Jan. 1995.

[2] Kastell, D., Horvath, T. J., and Eitelberg, G., "Nonequilibrium Flow Expansion Experiment Around a Blunted Cone," Proceedings of the Second European Symposium on Aerothermodynamics for Space Vehicles, ESA SP-367, Feb. 1995.

[3] Gochberg, L. A., Allen, G. A., Gallis, M. A., and Deiwert, G. S., "Comparison of Computations

and Experiments for Nonequilibrium Flow Expansions Around a Blunted Cone." AIAA Paper 96-0231. Jan. 1996.

[4]Muylaert. J.. Walpot. L.. Spel. M.. Tumino. G.. and Steijl, R.. "Non Equilibrium Computational Analysis of Blunt-Cone Experiments Performed in the LENS and HEG Facilities." AIAA Paper 96-2436. June 1996.

[5]Horvath. T. J.. McGinley, C. B.. and Hannemann. K.. "Blunt Body Near Wake Flow Field at Mach 6." AIAA Paper 96-1935, June 1996.

[6]Horvath, T. J. and Hannemann. K.. "Blunt Body Near Wake Flow Field at Mach 10." AIAA Paper 97-0986, Jan. 1997.

[7]Hollis, B. R. and Perkins, J. N., "Transition Effects on Heating in the Wake of a Blunt Body," AIAA Paper 97-2569, June 1997.

[8]Nance, R. P., Horvath, T. J., and Hassan, H. A., "Transition and Turbulence Modeling for Blunt-Body Wake Flows," AIAA Paper 97-2570, Jan. 1997.

[9]Robinson, D. F., Harris, J. E.. and Hassan. H. A.. "Unified Turbulence Closure Model for Wall Bounded and Free Shear Flows," *AIAA Journal.* Vol. 33. No. 12. Dec. 1995, pp. 2325–2331.

[10]Mack, L. M., "Boundary-Layer Linear Stability Theory," AGARD Report 709, June 1984.

[11]Ragab, S. A. and Wu, J. L., "Linear Instabilities in Two-Dimensional Compressible Mixing Layers," *Physics of Fluids A*, Vol. 1, No. 6, 1989, pp. 957–966.

[12]Dhawan, S. and Narasimha, R., "Some Properties of Boundary Layer Flow During Transition from Laminar to Turbulent Motion," *Journal of Fluid Mechanics*, Vol. 3, No. 4, 1958, pp. 418–436.

[13]Olynick, D. P. and Hassan, H. A., "A New Two-Temperature Dissociation Model for Reacting Flows," *Journal of Thermophysics and Heat Transfer.* Vol. 7. No. 4, October–December 1993, pp. 687–696.

[14]Roe, P. L., "Approximate Riemann Solvers, Parameter Vectors and Difference Schemes," *Journal of Computational Physics*, Vol. 43, 1981, pp. 357–372.

[15]van Leer, B., "Towards the Ultimate Conservative Difference Scheme. V. A Second Order Sequel to Godunov's Method," *Journal of Computational Physics*, Vol. 32, 1979, pp. 263–275.

[16]Yoon, S. and Jameson, A., "An LU–SSOR Scheme for the Euler and Navier-Stokes Equations," AIAA Paper 87-0600, Jan. 1987.

AIAA 99-0153

Turbulence Modeling of Shock-Dominated Flows with a k-ζ Formulation

Robert P. Nance and H. A. Hassan
North Carolina State University, Raleigh, NC

37th AIAA Aerospace Sciences Meeting and Exhibit
January 11-14, 1999 / Reno, NV

Turbulence Modeling of Shock-Dominated Flows
with a k-ζ Formulation

Robert P. Nance*
North Carolina State University. Raleigh. NC
H. A. Hassan†
North Carolina State University. Raleigh. NC

An examination of hypersonic turbulent flows where shock/boundary-layer interaction takes place is undertaken. A k-ζ stress model is developed and used to consider two experiments: a Mach 5 shock/boundary-layer interaction and a Mach 9.22 compression corner. The stress model, like the two-equation k-ζ model. assumes the validity of Morkovin's approximation. Both models show good agreement with data for the Mach 5 cases but poor agreement for the Mach 9.22 cases. It is concluded that the key to the prediction of hypersonic turbulence is the relaxation of Morkovin's hypothesis. Such relaxation requires the simultaneous consideration of additional equations governing the variances of density and temperature as well as their dissipation rates.

Nomenclature

C_f	Skin-friction coefficient
k	Turbulent kinetic energy
P_k	Production of turbulent kinetic energy
p	Pressure
$\overline{Q}$	Reynolds- or time-averaged value of Q
$\tilde{Q}$	Favre-averaged value of Q
q	Heat-transfer rate
Re	Reynolds number
T	Temperature
t_{ij}	Laminar stress tensor
U	Velocity magnitude
u_i	Velocity vector
β	Flow deflection angle. degrees
δ_{ij}	Kronecker delta
ε	Turbulent dissipation
μ	Dynamic viscosity
ν	Kinematic viscosity
ρ	Density
τ_{ij}	Reynolds stress tensor
ω_i	Vorticity vector
ζ	Enstrophy

Subscripts

d	Deviatoric component
T	Turbulent value
w	Wall value
∞	Freestream value

* Research Assistant. Currently: Postdoctoral Fellow. The Johns Hopkins University Applied Physics Laboratory. Member AIAA.
† Professor. Department of Mechanical and Aerospace Engineering. Associate Fellow AIAA.

Introduction

The interaction between a shock wave and turbulent boundary layer is one of the most significant fluid-dynamic problems currently facing designers of high-speed vehicles. Shock/boundary-layer interactions may be found in airbreathing inlets. at wing-body junctures, and on deflected control surfaces. Accurate characterization of these interactions. including resultant heat-transfer rates and prediction of separated regions. is very important for the design of efficient hypersonic flight configurations.

Attempts at modeling these types of interactions in hypersonic flows have not yet met with the success that has been achieved at lower speeds. The object of this investigation is to examine some of the limitations of existing model approaches. dispel some current misconceptions. and suggest ways to develop the models necessary for the accurate description of hypersonic turbulent flows. This discussion will be carried out in conjunction with two experiments that involve shock-induced separation. The first[1] is a well-documented experiment by Schülein et al. involving the interaction of an oblique shock wave with a Mach 5 turbulent flat-plate boundary layer. The second is an older experiment by Coleman et al.[2] at Mach 9.22. This particular dataset survived the scrutiny of Settles and Dodson.[3] The first experiment was the subject of a recent investigation by Lindblad et al.[4] using a variety of two-equation and algebraic stress models. The second experiment was examined by Grasso and Falconi[5] using a k-ε model.

The k-ζ model[6] will be used as the basis of this study. The model performs well for both free and wall-bounded shear flows with and without separation. It is free of damping and wall functions and is coordinate-independent. Moreover. modeled correlations are tensorially consistent and invariant under a Galilean transformation. The model is limited to flows where Morkovin's hypothesis[7] is expected to hold.

It has been suggested[8,9] that the inability of existing two-equation models to predict surface properties is a result of

the consideration that the turbulent kinetic energy production. P_k, is inversely proportional to the grid spacing normal to the shock. When this behavior is coupled with the fact that two-equation models do not accurately predict normal stresses even at low speeds, the production term in the k equation can assume inaccurate values. Incorrect prediction of this term will invariably lead to incorrect predictions of surface properties. As a result of this behavior, it is now a common practice to limit P_k to some multiple of the dissipation rate. That is, the definition

$$P_k \equiv \tau_{ij} \frac{\partial \tilde{u}_i}{\partial x_j} \qquad (1)$$

is often replaced with

$$P_k = \min \left\{ \tau_{ij} \frac{\partial \tilde{u}_i}{\partial x_j}, \, \bar{\lambda \rho \varepsilon} \right\} \qquad (2)$$

where τ_{ij} is the Reynolds stress tensor and λ is a user specified constant.

When a stress model is implemented, it is important to note that the integrated production of turbulent kinetic energy across a normal shock can be written as

$$\int \tau_{ij} \frac{\partial \tilde{u}_i}{\partial x_j} dt = \int \tau_{xx} \frac{\partial \tilde{u}}{\partial x} dt$$

$$\approx \tau_{xx} \left(\frac{\Delta \tilde{u}}{\Delta x} \right) \frac{\Delta x}{\tilde{u}}$$

$$\sim \tau_{xx} \qquad (3)$$

which is finite and grid-independent. This result would suggest that the key to accurately predicting surface properties in shock-dominated flows is to use stress models rather than two-equation models.

Based on the above considerations, a k-ζ based stress model is developed and used to study the experiments of References 1 and 2. The stress model was tested to ensure that it reproduces data for the incompressible flow over a flat plate and in its wake. Contrary to the prevailing wisdom, it is shown that the two-equation model behaves in a manner similar to that of the stress model: both perform well for the Mach 5 experiments, and both did poorly for the Mach 9.22 experiments. This finding was not much different from that of Zha and Knight,[10] who used a stress model to study a crossing-shock problem: its prediction of surface properties was not much better than the underlying two-equation model.

Based on this investigation, it appears that accurate predictions of strong shock/boundary-layer interactions requires the relaxation of Morkovin's hypothesis. This relaxation, in turn, requires supplementing existing turbulence models with equations governing the variances of density and/or temperature together with their respective dissipation rates.

Modeling Approach

In this work, we solve the Favre-averaged full Navier-Stokes equations for compressible two-dimensional flows. Closure is obtained through use of the two-equation k-ζ turbulence model and one of two methods for determining the normal Reynolds stresses.

k-ζ Model Equations

Turbulence length and time scales are provided in this work by the compressible k-ζ model first proposed by Robinson, Harris and Hassan.[11] The final version of the model equations is given in Ref. 6 and is also listed below. Model constants are listed in Table 1. The exact unmodeled k-ζ equations are given in the Appendix.

$$\bar{\rho} \frac{Dk}{Dt} = \tau_{ij} \frac{\partial \tilde{u}_i}{\partial x_j} + \frac{\partial}{\partial x_j} \left[\left(\frac{\mu}{3} + \frac{\mu_T}{\sigma_k} \right) \frac{\partial k}{\partial x_j} \right]$$
$$- \tilde{C}_1 \frac{\bar{\rho} k}{\tau_\rho} - \mu \zeta - \frac{1}{C_k} \frac{v_T}{\bar{\rho}} \frac{\partial \bar{\rho}}{\partial x_k} \frac{\partial \bar{p}}{\partial x_k} \qquad (4)$$

$$\bar{\rho} \frac{D\zeta}{Dt} = \frac{\mu_T}{\sigma_r} \frac{\partial \tilde{\omega}_i}{\partial x_j} \left[\left(\frac{\partial \tilde{\omega}_i}{\partial x_j} + \frac{\partial \tilde{\omega}_j}{\partial x_i} \right) \right]$$
$$+ \frac{\partial}{\partial x_j} \left[\left(\mu + \frac{\mu_T}{\sigma_\zeta} \right) \frac{\partial \zeta}{\partial x_j} \right] - \frac{\beta_5}{\sqrt{R_t} + \delta} \bar{\rho} \zeta^{\frac{3}{2}}$$
$$- \left[\alpha_3 B_{ij} + \frac{1}{3} \delta_{ij} \right] \bar{\rho} \zeta \tilde{s}_{ij} - \frac{\beta_4 \zeta \tau_{ij} \tilde{\omega}_i \tilde{\omega}_j}{k \tilde{\omega}}$$
$$- \frac{2 \beta_6 \tau_{ij} v_T}{kv} \tilde{\omega} \tilde{\omega}_i \tilde{\omega}_j + \frac{\beta_7 \bar{\rho} \zeta}{\tilde{\omega}^2} \tilde{\omega}_i \tilde{\omega}_j \tilde{s}_{ij}$$
$$- \max (P_\zeta, 0) - \frac{C_{\zeta 1} \mu_T \zeta \tilde{\omega}}{k \tau_0} - 2 \bar{\rho} \zeta \tilde{s}_{kk} \qquad (5)$$

where

$$\tau_{ij} = -\overline{\rho u_i' u_j'}, \qquad \omega_i = \varepsilon_{ijk} \frac{\partial \tilde{u}_k}{\partial x_j}$$

$$B_{ij} = \frac{\tau_{ij} + \frac{2}{3} \bar{\rho} k \delta_{ij}}{\bar{\rho} k}$$

$$s_{ij} = \frac{1}{2} \left(\frac{\partial \tilde{u}_i}{\partial x_j} + \frac{\partial \tilde{u}_j}{\partial x_i} \right)$$

$$k = \frac{1}{2} \widetilde{u_k' u_k'}; \quad \zeta = \widetilde{\omega_k' \omega_k'}; \quad \tilde{\omega}^2 = \tilde{\omega}_i \tilde{\omega}_i$$

$$R_t = \frac{k^2}{v \cdot \zeta}; \quad v_T = \frac{\mu_T}{\bar{\rho}}; \quad \mu_T = C_\mu \frac{k^2}{v \zeta}$$

$$P_\zeta = \bar{\rho} \frac{D\bar{p}}{Dt} \frac{k \tilde{\omega}}{v \bar{\rho} \sigma_p} \frac{1}{(1 + \delta_p)}$$

$$\delta_\rho = \frac{\sigma_\rho}{\bar{\rho}} \sqrt{\frac{2kR_t}{\zeta} \left(\frac{\partial \bar{\rho}}{\partial x_k} \right)^2}$$

2

$$\frac{1}{\tau_{ij}} = \frac{1}{\rho}\sqrt{\lambda(\partial\bar{\rho}/\partial x_i)^2}$$

As indicated above. Morkovin's hypothesis is employed in deriving the model equations (4) and (5) from the exact equations governing k and ζ (Eqs. A.1 and A.2 in the Appendix). According to this hypothesis, the pressure and total-temperature fluctuations are negligible for non-hypersonic boundary layers with *conventional rates of heat transfer*. Thus, all correlations involving p' in Eqs. (A.1) and (A.2) were ignored when deriving above model equations. Traditionally, Mach (M) 5 has been chosen as the Mach number below which Morkovin's approximation is expected to hold when considering wall-bounded shear flows. Thus, based on the above consideration, one should expect that current k-ζ formulation in either a stress or two-equation version, to perform well for wall bounded flows at $M=5$ or less, but not for higher Mach numbers. Above $M=5$, amplitudes of density and temperature fluctuations become significant and can not be ignored. Therefore, at hypersonic Mach numbers, equations governing variances of density and temperature together with their dissipation rates must be part of a turbulence model.

The stress model developed here again invokes Morkovin's approximation. This will facilitate assessment of performance of stress and two-equation models when used to solve a problem where Morkovin's approximation is expected to hold and where it is not expected to hold.

Reynolds Stress Closure

The Boussinesq approximation, i.e.,

$$\tau_{ij} \equiv -\overline{\rho u_i' u_j'} = \mu_T\left(2\tilde{s}_{ij} - \frac{2}{3}\delta_{ij}\tilde{s}_{kk}\right) - \frac{2}{3}\delta_{ij}\bar{\rho}k \quad (6)$$

has been widely used in turbulence modeling. This assumption generally yields good results for the shearing stress but not for the normal stresses, as is indicated in Fig. 1. This plot compares predicted root-mean-square (RMS) velocity fluctuations using the k-ζ model to the experimental data obtained by Klebanoff[12] for incompressible flow over a flat plate. Application of the thin-shear-layer approximation to Boussinesq's assumption yields purely isotropic normal stresses, such that

$$\tau_{xx} = \tau_{yy} = \tau_{zz} = -\frac{2}{3}\bar{\rho}k$$

Consequently, all three RMS fluctuation intensities follow a single curve, as demonstrated in Fig. 1. Clearly, the two-equation approach yields inaccurate results for the normal stresses even for this very simple flowfield. An alternative approach is to pursue a stress formulation. A differential stress model adds five equations to a two-equation model. This additional complexity and cost has discouraged potential users in the past and shifted attention to Algebraic Reynolds Stress Models (ARSM). These algebraic stress

models are derived from differential stress models by making two important assumptions: diffusion is negligible and turbulence is in equilibrium. Both of these assumptions are invalid for separated flows. Therefore, one should not expect ARSM to improve our predictive
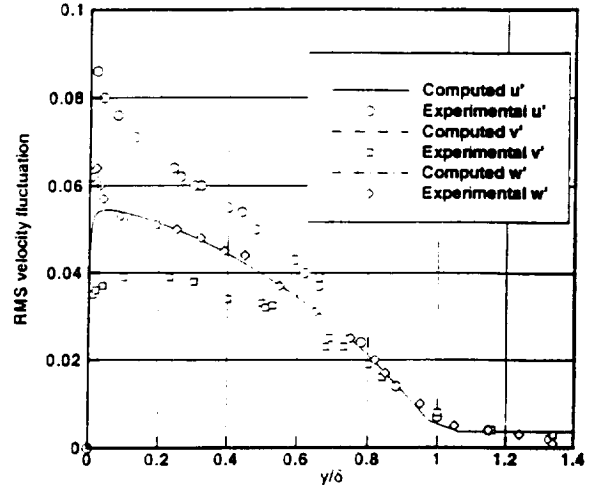

Fig. 1 Comparison of computed and experimental velocity fluctuations for flat-plate experiment of Klebanoff-two-equation model

capabilities of surface properties for such flows. This observation was confirmed by, among others, a recent investigation conducted by Rizzetta[13] in which he studied shock wave/boundary layer interactions using three ARSM, two two-equation models and an algebraic model. He concluded that ARSM offered little improvement over the other models.

A stress model based on the k-ζ formulation is developed here. In order to avoid the expense of employing a full stress model, all calculations presented here were based on a Partial Differential Stress (PDS) model. In this approach, the shear stress is calculated from a Boussinesq approximation while the normal stresses are calculated using modeled transport equations for these quantities. Thus, whether one deals with two- or three-dimensional flows, the overhead for this model is two additional field equations.

To formulate this new approach, we begin with the exact Reynolds stress equation[14]

$$\bar{\rho}\frac{DC_{ij}}{Dt} = -P_{ij} + \varepsilon_{ij} - \Pi_{ij} - D_{ij}$$

$$- \overline{u_i'}\frac{\partial\bar{p}}{\partial x_j} - \overline{u_j'}\frac{\partial\bar{p}}{\partial x_i} + \frac{2}{3}\overline{p'\frac{\partial u_m'}{\partial x_m}}\delta_{ij} \quad (7)$$

where

$$C_{ij} = \frac{\tau_{ij}}{\bar{\rho}}$$

3

$$P_{ij} = \tau_{ik} \frac{\partial \bar{u}_j}{\partial x_k} + \tau_{jk} \frac{\partial \bar{u}_i}{\partial x_k}$$

$$\varepsilon_{ij} = t_{kj} \frac{\partial u_i^*}{\partial x_j} + t_{ki} \frac{\partial u_j^*}{\partial x_k}$$

$$\Pi_{ij} = p' \left(\frac{\partial u_i^*}{\partial x_j} - \frac{\partial u_j^*}{\partial x_i} \right) - \frac{2}{3} p' \frac{\partial u_m^*}{\partial x_m} \delta_{ij}$$

$$D_{ij} = \frac{\partial}{\partial x_k} [\overline{t_{kj} u_i^* + t_{ki} u_j^*}$$

$$- (\rho u_i u_j u_k + \overline{p' u_i} \delta_{jk} + \overline{p' u_j} \delta_{ik})]$$

The second-order tensors ε_{ij} and D_{ij} may be decomposed into isotropic and deviatoric components. Thus,

$$\varepsilon_{ij} = \frac{2}{3} \bar{\rho} \varepsilon \delta_{ij} + \varepsilon_{ij,d}$$

$$D_{ij} = \frac{2}{3} \bar{\rho} D \delta_{ij} + D_{ij,d}$$

The exact Reynolds stress equation can then be rewritten as

$$\bar{\rho} \frac{DC_{ij}}{Dt} = -P_{ij} + \frac{2}{3} \bar{\rho} \varepsilon \delta_{ij} - \frac{2}{3} \bar{\rho} D \delta_{ij} - \Phi_{ij}$$

$$+ \overline{u_i'} \frac{\partial \bar{p}}{\partial x_j} + \overline{u_j'} \frac{\partial \bar{p}}{\partial x_i} - \frac{2}{3} \overline{p' \frac{\partial u_m^*}{\partial x_m}} \delta_{ij} \qquad (8)$$

where

$$\Phi_{ij} = D_{ij,d} - \varepsilon_{ij,d} - \Pi_{ij} \qquad (9)$$

Upon contraction, Eq. (8) reduces to Eq. (A.1) in the Appendix. Therefore, assumptions that were used in modeling the k equation can be adopted here. This ensures that the underlying k-ζ formulation is the same for both the two-equation and the stress model. An added advantage is that the only term that requires modeling is Φ_{ij}. Hence, the model Reynolds stress equation is

$$\bar{\rho} \frac{DC_{ij}}{Dt} = - \left(\tau_{ik} \frac{\partial \bar{u}_j}{\partial x_k} + \tau_{jk} \frac{\partial \bar{u}_i}{\partial x_k} \right)$$

$$+ \frac{2}{3} \left(\mu \zeta + \bar{C}_1 \frac{\bar{\rho} k}{\tau_\rho} \right) \delta_{ij}$$

$$- \frac{2}{3} \frac{\partial}{\partial x_m} \left[\left(\frac{\mu}{3} + \frac{\mu_T}{\sigma_k} \right) \frac{\partial k}{\partial x_m} \right] \delta_{ij}$$

$$+ \frac{1}{C_k} \frac{\nu_T}{\bar{\rho}} \left(\frac{\partial \bar{\rho}}{\partial x_i} \frac{\partial \bar{p}}{\partial x_j} - \frac{\partial \bar{\rho}}{\partial x_j} \frac{\partial \bar{p}}{\partial x_i} \right)$$

$$- \Phi_{ij} \qquad (10)$$

Consistent with the practice employed in developing the k-ζ model,[6,11] the quantity Φ_{ij} will be modeled to be a linear combination of the anisotropy tensor, b_{ij}, and its derivatives. The resulting expression can be written as

$$\frac{\Phi_{ij}}{\bar{\rho}} = - C_1 \varepsilon b_{ij} + C_2 k S_{ij}^*$$

$$- C_3 k \left[b_{il} S_{jl}^* + b_{jl} S_{il}^* - \frac{2}{3} b_{mn} S_{mn}^* \delta_{ij} \right]$$

$$+ C_4 k [b_{il} W_{jl} + b_{jl} W_{il}]$$

$$+ \frac{\partial}{\partial x_m} \left[(\nu + C_5 \nu_T) \frac{\partial (k b_{ij})}{\partial x_m} \right] \qquad (11)$$

with

$$b_{ij} = - \frac{C_{ij} + \frac{2}{3} k \delta_{ij}}{2k}, \qquad \varepsilon = \nu \zeta$$

$$S_{ij}^* = \frac{1}{2} \left[\frac{\partial \bar{u}_i}{\partial x_j} + \frac{\partial \bar{u}_j}{\partial x_i} \right] - \frac{1}{3} \frac{\partial \bar{u}_m}{\partial x_m} \delta_{ij}$$

$$W_{ij} = \frac{1}{2} \left[\frac{\partial \bar{u}_i}{\partial x_j} - \frac{\partial \bar{u}_j}{\partial x_i} \right]$$

Note that each model term contracts to zero independently.

The constants $C_1 - C_4$ can depend on the invariants of b_{ij} and $P_k / \bar{\rho} \varepsilon$. As a first step they will be treated as constants. They will be determined from rapid distortion theory, which gives C_2, and the rest from Laufer's experiment in channels.[15] Rapid distortion theory gives

$$\lim_{b_{ij} \to 0} \Phi_{ij} = 0.8 \bar{\rho} k S_{ij}^*$$

which gives

$$C_2 = 0.8 \qquad (12)$$

Laufer's measurements give, in the log-law region where $P_k / \bar{\rho} \varepsilon = 1$,

$$b_{11} = 0.22, \quad b_{22} = -0.15, \quad b_{12} = -0.15 \qquad (13)$$

Equations (12) and (13) yield

$$C_1 = 2.513, \quad C_3 = 1.473, \quad C_4 = 1.07 \qquad (14)$$

An adjustment of the above model constants is required for situations where $P_k / \bar{\rho} \varepsilon \neq 1$. Abid and Speziale[16] have suggested that second order closures should yield approximately equal equilibrium values for b_{ij} for both

homogeneous shear flows and the log-law region. This goal can be achieved by a simple modification of C_1 to

$$C_1 = 2.0 + 0.513 (P_k / \overline{\rho}\varepsilon) \qquad (15)$$

(Note that C_1 here is $2C_1$ in Ref. 16.) The above choice replaces Rotta's constant by 2.0 and results in homogeneous shear flow values of b_{ij} that are given by Eq. (13) for all values of $P_k / \overline{\rho}\varepsilon$ [see Eq. (11) in Ref. 16.]

The constant C_5 was chosen so as to reproduce correct skin friction for a flat plate. Thus, the model constants for low speed flows in the absence of adverse pressure gradients can be summarized as

$$C_1 = 2.0 + 0.513(P_k/\overline{\rho}\varepsilon), \quad C_2 = 0.8, \quad C_3 = 1.473,$$
$$C_4 = 1.07, \quad C_5 = 0.1 \qquad (16)$$

Again, consistent with the development of the k-ζ model, the role of compressibility and adverse pressure gradients had to be addressed. From study of shock wave/boundary layer interaction, C_1 was multiplied by the factor

$$\left\{ \frac{1 - \beta_\rho \tau_u / \tau_\rho}{1 + \frac{\beta_p}{\mu\zeta} \cdot \max\left[\frac{D\overline{p}}{Dt}, 0 \right]} \right\}$$

where

$$\frac{1}{\tau_u} = \sqrt{\overline{s}^2 + \tilde{\omega}^2 / 2} \qquad (17)$$

The model constants β_p and β_ρ, as well as the other stress model constants, are listed in Table 2.

Table 1 k-ζ / PDS model constants

Constant	Value
C_μ	0.09
α_3	0.35
β_4	0.42/0.39
β_5	2.37
β_6	0.10/0.18
β_7	1.50
σ_p	0.065
σ_r	0.07
σ_ρ	65.0
$1/\sigma_k$	1.80
$1/\sigma_\zeta$	1.46
δ	0.10
$\tilde{C}_1$	0.60
C_k	1.00
C_{ζ_1}	2.10

Table 2 PDS model constants

Constant	Value
C_1	$2 + 0.513\ P_k /(\overline{\rho}\varepsilon)$
C_2	0.8
C_3	1.473
C_4	1.07
C_5	0.10
β_p	0.18
β_ρ	0.57

Note that, in developing this model, we preserved all the desirable features of the two-equation model, including avoidance of wall or damping functions and coordinate independence. Moreover, all correlations are tensorially consistent and Galilean invariant. Further, as shown in Table 1 the majority of the k-ζ constants remain unchanged for the PDS model. The constants β_4 and β_6, however, are modified slightly as shown.

Numerical Method

The modeling proposed here has been incorporated into Olynick and Hassan's[17] two-dimensional/axisymmetric implicit solver for hypersonic flows. This algorithm solves the governing equations for 5-species air in thermochemical nonequilibrium. The solver uses Roe's flux-difference splitting[18] for the inviscid flux, extended to higher order using MUSCL variable extrapolation[19] with a minmod slope limiter. Time integration is accomplished using the diagonal implicit variant of Yoon and Jameson's Lower-Upper Symmetric Gauss-Seidel method,[20] which only requires the inversion of diagonal matrices. This property is attractive for nonequilibrium flows, where a large number of partial defferential equations must be solved.

Since the current flowfields under investigation are perfect-gas, vibrational relaxation and chemical reactions are disabled to obtain the results in this study. Additionally, the high-temperature transport-property calculations originally used in the code were replaced with Sutherland's law for viscosity and a constant laminar Prandtl number of 0.72. Closure for the Favre-averaged energy equation is accomplished using a constant turbulent Prandtl number of 0.89.

Results and Discussion

Before considering high Mach number flows, it is worthwhile to examine the performance at the PDS model for low speed flows in the absence of adverse pressure gradients. This study will help evaluate the choice of model constants indicated in Eq. (16). A flat plate and its wake were selected for this validation. Of the many results that were generated, two critical comparisons will be presented. Figure 2 compares computed RMS velocity

5

fluctuations with Klebanoff's experiment.[2] while Fig. 3 compares computed wake growth rate with those of the two-equation k-ζ model[6] and the experiments of Pot[21] and Weygandt and Mehta.[22] In Fig. 3, b is the half width, θ is the momentum thickness and x is the distance along the wake. As is seen in the figures, good agreement is indicated in both cases.

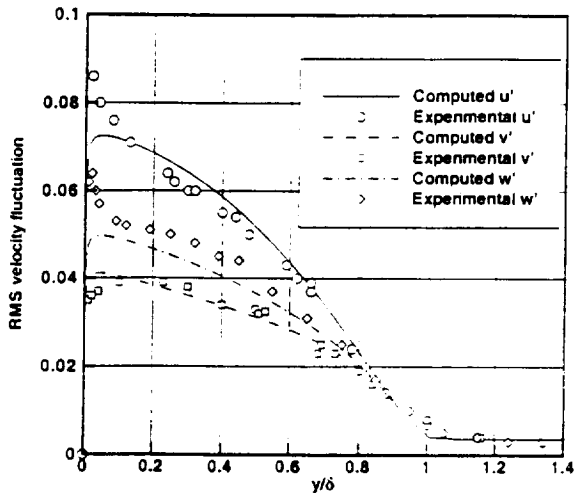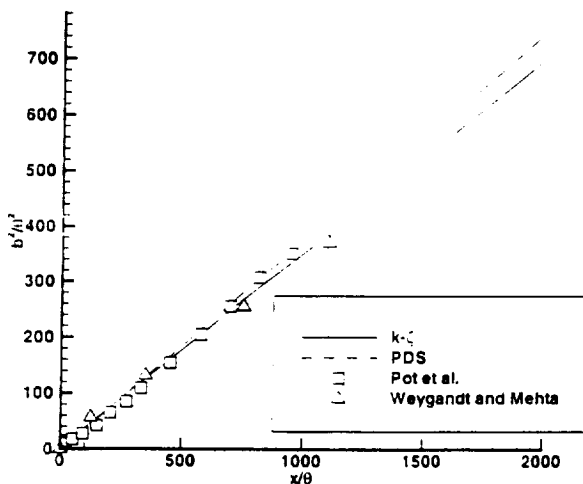**Fig. 2   Comparison of computed and experimental velocity fluctuations for flat-plate experiment of Klebanoff-PDS model**

Fig. 3   Comparison of k-ζ and PDS results for incompressible flat-plate wake

We shall consider next two different classes of shock/boundary-layer interaction flowfields, including Mach 5 impingement of an oblique shock wave and the flow past a compression corner at Mach 9.22. These computations correspond to experiments conducted by Schülein et al.[1] and Coleman et al.,[2] respectively. It should be noted that the first experiment was completed after Settles and Dodson completed their examination of

available data sets for code validation. However, the experiment met all their guidelines. The work of Coleman et al. was on their list of recommended experiments. Note that, for each of the computations presented here, the leading edge of the flat plate or compression ramp is not included in the Navier-Stokes computations. Instead, inflow profiles are obtained separately through boundary-layer solutions for the corresponding zero-pressure-gradient flat-plate flow.

Computations for Schülein et al. Cases

First, we shall examine a Mach 5 shock/boundary-layer interaction modeled using the experimental setup shown in Fig. 4. A shock generator is mounted on the upper tunnel wall, and the resultant oblique shock wave interacts with the turbulent boundary layer growing on the flat plate along the lower tunnel wall. Depending on the magnitude of the
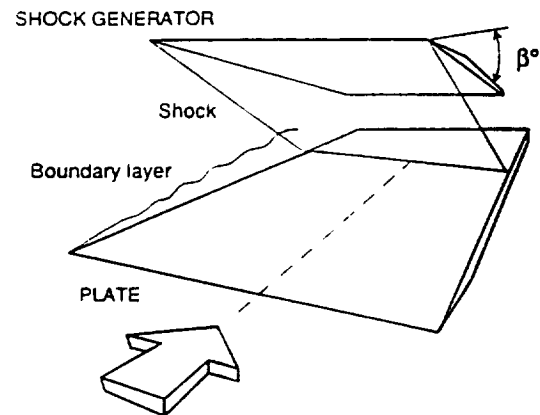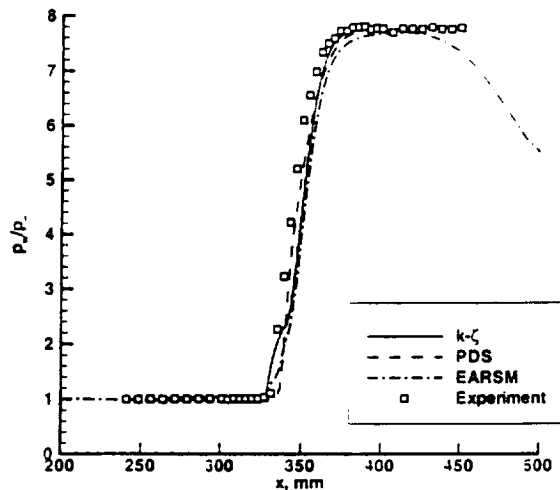

Fig. 4   Schematic of shock/boundary-layer interaction experiment performed by Schülein et al.

deflection angle β, flow separation may or may not occur at the location of shock impingement. We consider two values of β which result in separated flow. The oblique shock is enforced numerically by enforcing velocity, pressure, temperature and density boundary conditions along the top of the computational domain that correspond to the conditions behind the oblique shock. It was indicated in Ref. 4 that an 80 × 80 grid resulted in a well resolved solution. Therefore, in order to ensure a grid-resolved result, all present computations were conducted on a 141 × 141 Cartesian grid with constant spacing in the x direction and geometric spacing in the y direction.
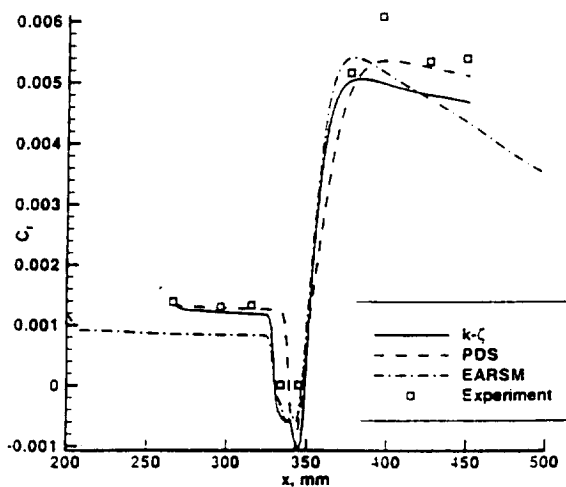
Before detailed comparisons are undertaken, the turbulence model of Ref. 4 will be reviewed. Lindblad et al.[4] employed a number of two-equation, ARSM and differential stress models in their investigation. We will be comparing here with what they considered to be their best performing model, which happened to be an Explicit Algebraic Reynolds Stress Model (EARSM) with the underlying two-equation model being the k-ω model of Wilcox. This EARSM is based on the ARSM of Rodi[23] and the pressure-strain model of Launder et al.[24] A near

wall treatment. which included damping functons. was then added[25,26] to allow the Reynolds stress anisotropy to behave in accordance with experiment and direct numerical simulation. Evidently,[4] compressibility corrections as suggested in Refs. 27 and 28 were deemed unimportant and thus. none were included.

Fig. 5 compares nondimensional surface pressure and skin-friction results obtained with the standard k-ζ model and the PDS model to the experimental measurements of Schülein et al. for $\beta = 10°$. Also shown are the results obtained by Lindblad et al.[4] using an EARSM for the same case. Fig. 5(a) shows that the present computations both predict the downstream pressure quite well. but offer differing results in the interaction region. These differences appear to arise because of a considerably smaller separation zone predicted by the PDS model. as indicated in Fig. 5(b). Outside the interaction region.

however. all models compare quite well to the experimental skin-friction data. For this case, the agreement appears to be better than that provided by the EARSM computation.

Fig. 6 shows that the agreement is generally poorer for the case where $\beta = 14°$. For instance, the present two-equation computation predicts the general behavior of the pressure distribution quite well; however, it underpredicts the pressure in the interaction region and shows an overprediction in the downstream equilibrium region. The PDS model better predicts the downstream pressure but does not agree well in the interaction region. For the skin friction. the PDS model appears to match the skin-friction data better than the standard k-ζ approach. but predicts later separation and reattachment. It is also clear that both the standard k-ζ model and the EARSM calculation yield large overpredictions of the skin friction in the recovery

a)Pressure distribution

b) Skin-friction distribution

Fig. 5 Results for experiments of Schülein et al.. $\beta = 10°$
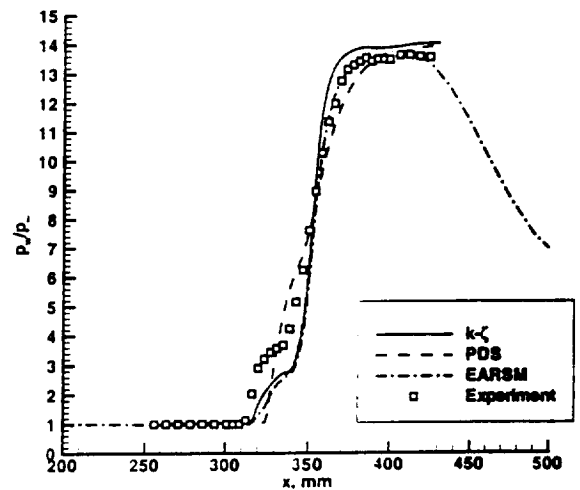
a)Pressure distribution
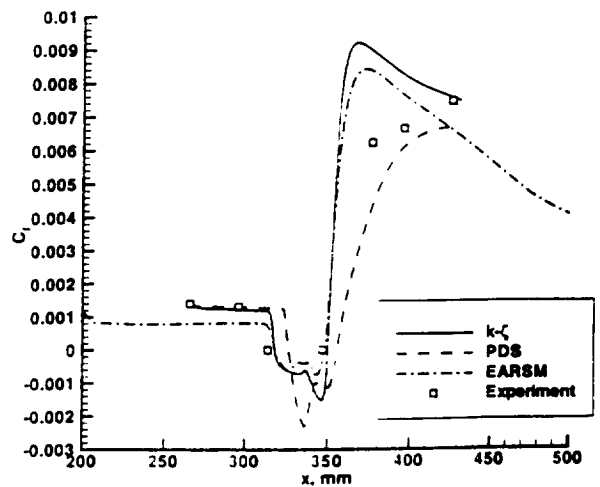
b) Skin-friction distribution

Fig. 6 Results for experiments of Schülein et al., $\beta = 14°$

region. Overall. the k-ζ and PDS calculations provide similar degrees of predictive accuracy for these Mach 5 cases.

It is to be noted that. in all of our calculations presented here. no attempt was made to limit the ratio of production to dissipation. Detailed investigation of results from the two-equation model indicated that. in regions where production over dissipation was unusually high, production was dominated by normal stresses. This may be the reason why skin friction was overpredicted in the recovery region by the two-equation model.

Computations for Coleman et al. Cases

The second set of experiments considers the flow past a two-dimensional compression corner in a Mach 9.22 freestream. For these cases. we shall compare computational results to experimental surface-pressure and heat flux results obtained by Coleman et al.[2] A representative computational grid for one of the two deflection angles considered is shown in Fig. 7. The minimum grid spacing at the wall decreases linearly from the inflow plane to the corner. after which point it is constant. Two flow deflection angles. $\beta = 34°$ and $\beta = 38°$, are examined for this case as well; flow separation is expected for both deflection angles. Both the 34- and 38-degree grids employed 241 points in the streamwise direction and 141 points in the normal direction. This is comparable to 256×128 grid employed in Ref. 5. which resulted in a grid-independent solution.
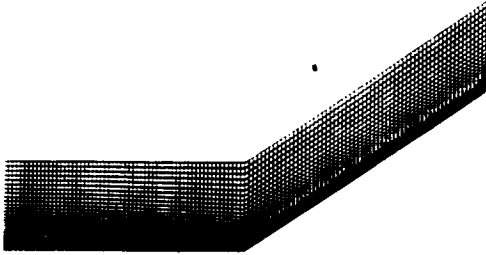

Fig. 7 241×141 grid for Coleman et al. experiment. $\beta = 34°$. Every other grid point omitted for clarity.

The calculations of Ref. 5 were based on a two-equation k-ε model with a number of compressibility corrections involving terms appearing in the k equation. and the Karman constant. Moreover. the eddy viscosity definition was adjusted so as to limit the turbulent length scale.

As indicated earlier. because all correlations involving p' were set to zero. our model is not expected to perform well for the M=9.22 case. The need to include temperature

and density fluctuations can be seen when one considers. as an example. the pressure dilatation term $\overline{p'u_{i,i}'}$. Since

$$p = \bar{p} + p' = R\rho(\bar{T} + T')$$

$$p' = R(\rho'\bar{T} + \rho T')$$

and

$$\overline{p'u_{i,i}'} = R[\bar{T} \overline{\rho'u_{i,i}'} + \bar{\rho} \overline{T'u_{i,i}'}],\qquad(19)$$

it is not obvious why the above term should be modeled in terms of turbulent kinetic energy production P_k and its dissipation rate $\bar{\rho}\varepsilon$, as suggested by Sarkar[28] and used in Ref. 5. We believe that appropriate modeling of terms appearing in Eq. (19) must depend on the variances of temperature and density and their dissipation rates.

We shall first compare predictions for inflow properties with these of Ref. 5 and experiment. These results are shown in Fig. 8. Fig. 8(a) shows that both the k-ζ solution and the PDS solution match experimental velocity-profile data better than the earlier calculation. In the case of the Mach-number distribution (Fig. 8(b)), the Grasso and Falconi result agrees better with the data in the outer region, but the present computations are superior in the near-wall region.

It is seen from Fig. 8 that, in general, current predictions are better than those of Ref. 5 and in good agreement with experiment. The question arises as to why a theory that is not supposed to be valid in this Mach number range gives good agreement with experiment. This is because Morkovin's hypothesis requires *conventional heat transfer rates* which is the case for the inflow region. This is to be contrasted to the corner region. where high Mach numbers and unconventional rates of heat transfer exist.

The next two figures show pressure and heating results for the two deflection angles considered here. Fig. 9 compares the present results to the computations of Grasso and Falconi and experimental data for $\beta = 34°$. As demonstrated in Fig. 9(a), the present k-ζ computation appears to provide the best comparison with the experimental pressure data for this case, whereas the PDS result provides the worst agreement. On the other hand, the k-ε solution by Grasso and Falconi agrees fairly well with the experimental heat-transfer data. but both present computations provide substantial overpredictions of the peak heat-transfer rate. Note that the k-ζ result agrees with the data fairly well upstream and downstream of the interaction region; however. the predicted peak heat flux is more than twice that observed in the experiment. The PDS heating result overpredicts the heating in and downstream of the interaction region.

Similar behavior is observed for $\beta = 38°$ in Fig. 10(a); both the k-ζ and k-ε solutions predict the peak pressure magnitude quite well. Once again. however, the computation by Grasso and Falconi provide reasonable predictions of the heat-transfer rate. while both present computations overpredict the peak heating substantially.

8

Moreover, the PDS result again agrees poorly with the data downstream of the interaction region.

Concluding Remarks

This work extended the two-equation k-ζ turbulence closure model to a stress model and, in the process, preserved all the desirable features of the original model, i.e., no wall or damping functions, coordinate independence, Galilean invariance and tensorial consistency.

The above results illustrate the importance of using a turbulence model that reflects the correct physics of the problem. The k-ζ model worked for the Mach 5 shock wave/boundary-layer interactions and for the 9.22 flat-plate boundary-layer computations. However, it did not provide accurate predictions for the separation zone in the Mach 9.22 compression-corner flowfields. As a result, we believe that the key to developing accurate models for hypersonic turbulence is to relax Morkovin's approximation and provide adequate modeling for terms neglected in Eqs. (A.1) and (A.2). Replacing a two-equation model with a stress model is not going to lead to improved predictions if the underlying physics is inaccurate.

Another conclusion that may be drawn from this work is that, if the objective is to calculate surface properties, then two-equation models perform as well as stress models as long as the production term P_k is not dominated by contributions of normal stresses.

Finally, the fact that the PDS model underperformed the two-equation model for the Mach 9.22 compression ramp was unexpected. Future work should include comparison
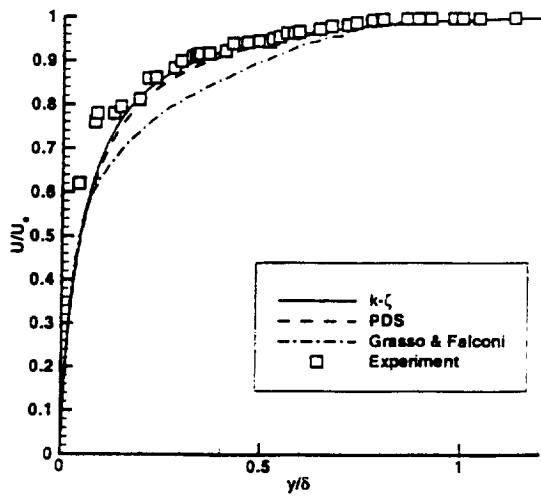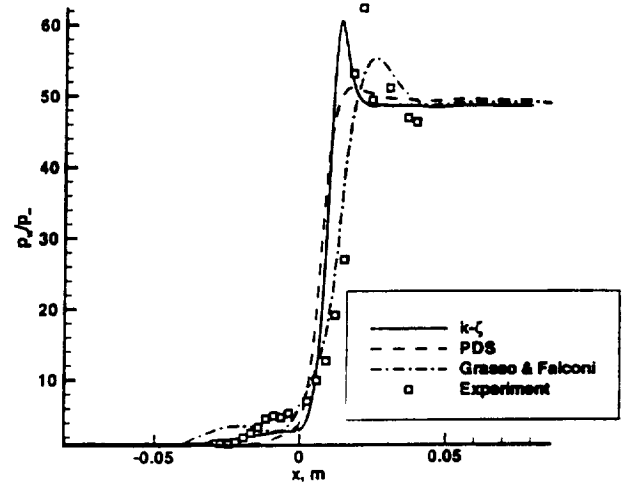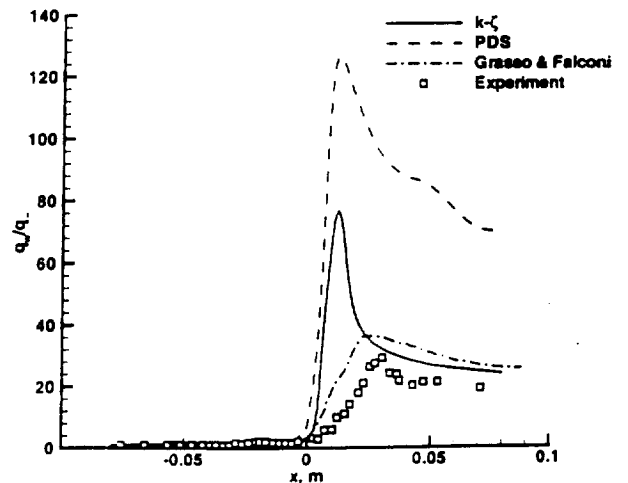

a) Velocity profile
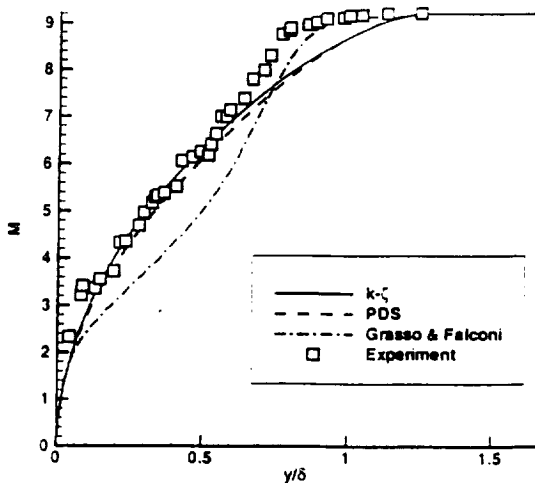
c) Mach-number profile

Fig. 8 Comparison of inflow profiles for experiment of Coleman et al.
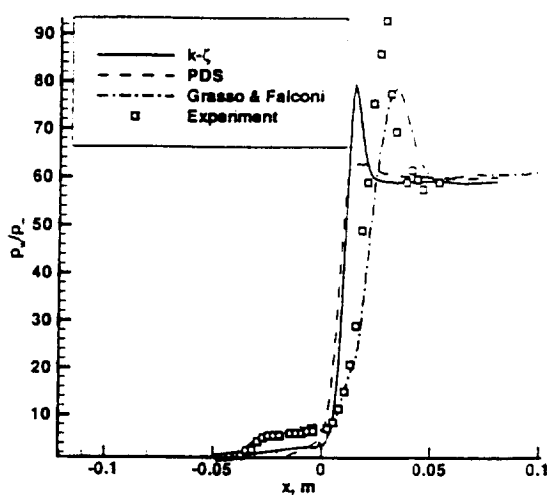

a) Pressure distribution

b) Heat-transfer distribution

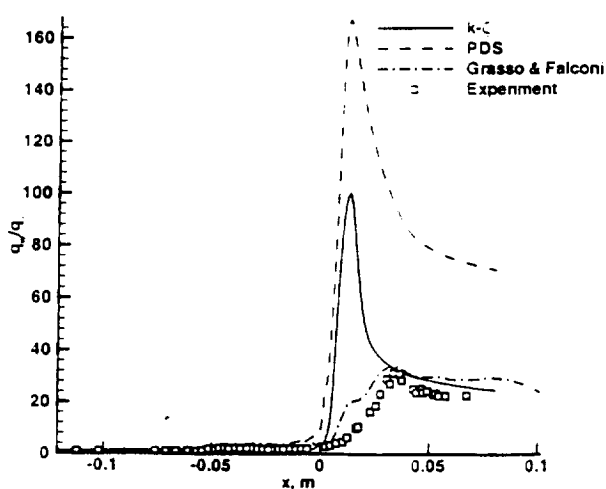Fig. 9 Results for experiments of Coleman et al., $\beta = 34°$

9

of the PDS model with a full stress mouel.

a) Pressure distribution

b) Heat-transfer distribution

Fig. 10 Result for experiments of Coleman et al., $\beta = 38°$

References

[1]Schülein. E.. Krogmann. P.. and Stanewsky, E.. "Documentation of Two-Dimensional Impinging Shock/Boundary Layer Interaction Flow." DLR Report IB 223-96 A 49. Oct. 1996.

[2]Coleman, G. T. and Stollery, J. L.. "Heat Transfer from Hypersonic Turbulent Flow at a Wedge Compression Corner." *Journal of Fluid Mechanics*. Vol. 56, No. Pt. 4, 1972, pp. 741-752.

[3]Settles. G. S. and Dodson. L. J.. "Supersonic and Hypersonic Shock/Boundary-Layer Interaction Database," *AIAA Journal*. Vol. 32, No. 7, July 1994, pp. 1377-1383.

[4]Lindblad. I. A. A., Wallin, S., Johansson, A. V., Friedrich, R., Lechner, R., Krogmann, P., Schülein, E., Courty, J.-C., Ravachol, M.. and Giordano, D., "A Prediction Method for High Speed Turbulent Separated Flows with Experimental Verification." AIAA Paper 98-2547, June 1998.

[5]Grasso. F. and Falconi, R., "High-Speed Turbulence Modeling of Shock-Wave/Boundary-Layer Interaction," *AIAA Journal*, Vol. 31, No. 7, July 1993, pp. 1199-1206.

[6]Robinson, D. F. and Hassan, H. A., "Further Development of the k-ζ (Enstrophy) Turbulence Closure Model." *AIAA Journal*, Vol. 36, No. 10, October 1998, pp. 1825-1833.

[7]Morkovin, M., "Effects of Compressibility on Turbulent Flows," *Mecanique de la Turbulence*, edited by A. Favre, CNRS, Gordon and Beach, 1964, pp. 367-380.

[8]Knight, D. D. and Degrez, G., "Shock Wave Boundary Layer Interactions in High Mach Number Flows. A Current Survey of Current CFD Prediction Capabilities," AGARD Working Group 18, 1997.

[9]Knight, D. D., "Simulation of Shock Wave–Turbulent Boundary Interactions Using the Reynolds–Averaged Navier-Stokes Equations," in *Proceedings of the ICASE/LaRC/AFOSR Symposium on Modeling of Complex Turbulent Flows*, Kluwer Academic Publishing, 1998.

[10]Zha. G.-C. and Knight, D. D., "Three-Dimensional Shock/Boundary-Layer Interaction Using Reynolds Stress Equation Turbulence Model." *AIAA Journal*, Vol. 34, No. 7. July 1996. pp. 1313-1320.

[11]Robinson. D. F.. Harris. J. E.. and Hassan, H. A., "Unified Turbulence Closure Model for Wall Bounded and Free Shear Flows." *AIAA Journal*, Vol. 33, No. 12, Dec. 1995, pp. 2325-2331.

[12]Klebanoff. P. S.. "Characteristics of Turbulence in a Boundary Layer with Zero Pressure Gradient," NACA Report TN-3178, 1956.

[13]Rizzetta. D. P.. "Evaluation of Explicit Algebraic Reynolds-Stress Models for Separated Supersonic Flows," *AIAA Journal*. Vol. 36, No. 1, January 1998, pp. 24-30.

[14]Wilcox. D. C.. *Turbulence Modeling for CFD*, DCW Industries. La Canada. CA. 1993.

[15]Laufer. J.. "Investigation of Turbulent Flow in a Two-Dimensional Channel." NACA Tech. Rept. 1053, 1951.

[16]Abid. R. and Speziale. C. G.. "Predicting Equilibrium States with Reynolds Stress Closures in Channel Flow and Homogeneous Shear Flow." *Physics of Fluids*. Vol. 5, No. 7. pp. 1776-1782, 1993.

[17]Olynick. D. P. and Hassan. H. A.. "A New Two-

Temperature Dissociation Model for Reacting Flows." *Journal of Thermophysics and Heat Transfer.* Vol. 7, No. 4, October-December 1993, pp. 687-696.

[18]Roe, P. L., "Approximate Riemann Solvers. Parameter Vectors and Difference Schemes." *Journal of Computational Physics.* Vol. 43, 1981, pp. 357-372.

[19]van Leer, B., "Towards the Ultimate Conservative Difference Scheme. V. A Second Order Sequel to Godunov's Method," *Journal of Computational Physics.* Vol. 32, 1979, pp. 263-275.

[20]Yoon, S. and Jameson, A., "An LU-SSOR Scheme for the Euler and Navier-Stokes Equations." AIAA Paper 87-0600, Jan. 1987.

[21]Pot, P. J. "Measurement in a Two-Dimensional Wake and in a Two-Dimensional Wake Merging into a Boundary Layer." NLR, TR-790634, The Netherlands, 1979.

[22]Weygandt, J. H. and Mehta, R. D., "Asymptotic Behavior of a Flat Plate Wake," NASA CR-185917, 1989.

[23]Rodi, W., "A New Algebraic Relation for Calculating Reynolds Stresses," Z *Angew-Math. Mech.,* Vol. 56, 1976, pp. 219-221.

[24]Launder, B. E., Reece, G. J., and Rodi, W., "Progress in the Development of a Reynolds-Stress Turbulence Closure," *Journal of Fluid Mechanics,* Vol. 68, Pt. 3, 1975, pp. 537-566.

[25]Wallin, S. and Johansson, A. V., "A Complete Explicit Algebraic Reynolds Stress Model for Incompressible and Compressible Turbulent Flows," Rept. FFA TN 1997-51, The Aeronautical Research Institute of Sweden, November, 1997.

[26]Wallin, S, Lechner, R. and Ravachol, M., "Implementation of a New EARSM into Different N-S Solvers," Rept. FFA TN 1997-13, The Aeronautical Research Institute of Sweden, April 1997.

[27]Sarkar, S., Erlebacher, G., Hussaini, M. Y., and Kreiss, H. O., "The Analysis and Modeling of Dilatational Terms in Compressible Turulence." *Journal of Fluid Mechanics.* Vol. 227, Part 2, 1991, pp. 473-493.

[28]Sarkar, S., "The Pressure-Dilatation Correlation in Compressible Flows," *Physics of Fluids A. Fluid Dynamics.* Vol. 4, No. 12, December 1992, pp. 2675-2682.

Appendix: Exact Equations Governing k and ζ

The exact Favre averaged compressible turbulence kinetic energy and enstrophy equations can be written as

$$\frac{\partial}{\partial t}(\bar{\rho}k) + \frac{\partial}{\partial x_j}(\bar{\rho}\tilde{u}_j k) = \tau_{ij}\frac{\partial \tilde{u}_i}{\partial x_j} - \bar{\rho}\varepsilon - \overline{u_i''}\frac{\partial \bar{p}}{\partial x_i} + \overline{p'\frac{\partial u_i''}{\partial x_i}}$$
$$+ \frac{\partial}{\partial x_j}\left[\overline{t_{ji}u_i''} - \frac{\overline{\rho u_j'' u_i'' u_i''}}{2} - \overline{p'u_j''}\right] \quad (A.1)$$

$$\frac{\partial}{\partial t}\left(\bar{\rho}\omega_i''^2\right) + \frac{\partial}{\partial x_k}\left(\bar{\rho}\tilde{u}_k\omega_i''^2 + 2\tilde{\omega}_i\,\overline{\rho u_k''\omega_i''} + \overline{\rho u_k''\omega_i''^2}\right)$$

$$- 2\tilde{\omega}_i\frac{\partial}{\partial x_k}(\overline{\rho u_k''\omega_i''}) = 2\left(\tilde{\omega}_m\,\overline{\rho\omega_i''s_{im}''} + \tilde{s}_{im}\,\overline{\rho\omega_i''\omega_m''}\right.$$

$$+ \overline{\rho\omega_i''\omega_m''s_{im}''} - \overline{\rho s_{kk}''\omega_i''^2} - \tilde{\omega}_i\,\overline{\rho\omega_i''s_{kk}''} - \left.\overline{\rho s_{kk}''\omega_i''^2}\right)$$

$$+ 2\frac{\varepsilon_{ijk}}{\bar{\rho}}\left[\frac{\partial\bar{\rho}}{\partial x_j}\,\overline{\omega_i''\left(\frac{\partial p'}{\partial x_k} - \frac{\partial t_{km}'}{\partial x_m}\right)}\right.$$

$$+ \overline{\omega_i''\frac{\partial p'}{\partial x_j}\left(\frac{\partial\bar{p}}{\partial x_k} - \frac{\partial\bar{t}_{km}}{\partial x_m}\right)} + \overline{\omega_i''\frac{\partial p'}{\partial x_j}\left(\frac{\partial p'}{\partial x_k} - \left(\frac{\partial t_{km}'}{\partial x_m}\right)\right)}$$

$$+ \left.\overline{\bar{\rho}\omega_i''\frac{\partial^2 t_{km}'}{\partial x_j\partial x_m}}\right] \quad (A.2)$$

$$s_{ij}'' = \frac{1}{2}\left(\frac{\partial u_i''}{\partial x_j} + \frac{\partial u_j''}{\partial x_i}\right), \qquad \tilde{s}_{ij} = \frac{1}{2}\left(\frac{\partial\tilde{u}_i}{\partial x_j} + \frac{\partial\tilde{u}_j}{\partial x_i}\right)$$

$$\tilde{\omega}_i = \varepsilon_{ijk}\frac{\partial\tilde{u}_k}{\partial x_j}, \qquad \omega_i'' = \varepsilon_{ijk}\frac{\partial u_k''}{\partial x_j}$$

$$k = \widetilde{u_i''u_i''}/2, \qquad \zeta = \widetilde{\omega_i''\omega_i''}, \qquad \tau_{ij} = -\overline{\rho u_i''u_j''} \quad (A.3)$$

$$t_{ij} = 2\mu s_{ij} - \frac{2}{3}\mu\frac{\partial u_k}{\partial x_k}\delta_{ij}, \qquad u_i = \tilde{u}_i + u_i'' = \bar{u}_i + u_i', \qquad v = \frac{\mu}{\rho}$$

National Aeronautics and
Space Administration

Langley Research Center
Hampton, VA 23681–0001

Reply to Attn of 408A

October 21, 1999

NASA Center for AeroSpace Information (CASI)
Parkway Center
7121 Standard Drive
Hanover, MD 21076-1320

Enclosed is a copy of the final report for NASA Cooperative Agreement NCC1-112. This report was filed with me on October 28, 1998 but according to the NASA Langley Research Center Grant Officer, no copy was sent to your organization.

If you have any questions concerning this report, please contact me at E-mail address r.g.wilmoth@larc.nasa.gov or by phone (757)-864-4368.

Sincerely,

Richard G. Wilmoth
Aerothermodynamics Branch

encl: